ACCEPTED MANUSCRIPT

Oncogenic KRAS Reduces Expression of FGF21 in Acinar Cells to Promote Pancreatic Tumorigenesis in Mice on a High-Fat Diet

Short Title: FGF21 as a downstream target of oncogenic KRAS

Yongde Luo[1,2,*], Yaying Yang[3,*], Muyun Liu[3,*], Dan Wang[2], Feng Wang[4], Yawei Bi[2], Juntao Ji[2], Suyun Li[2], Yan Liu[5], Rong Chen[6], Haojie Huang[5], Xiaojie Wang[1], Agnieszka K. Swidnicka-Siergiejko[5], Tobias Janowitz[7], Semir Beyaz[7], Guoqiang Wang[2], Sulan Xu[2], Agnieszka B. Bialkowska[2], Catherine K. Luo[2], Christoph L. Pin[8], Guang Liang[1], Xiongbin Lu[9], Maoxin Wu[10], Kenneth R. Shroyer[10], Robert A. Wolff[3], William Plunkett[6], Baoan Ji[11], Zhaoshen Li[12], Ellen Li[2], Xiaokun Li[1], Vincent W. Yang[2], Craig D. Logsdon[3,5,§], James L. Abbruzzese[3,13,§] & Weiqin Lu[2,3,§]

[1]School of Pharmaceutical Science, Wenzhou Medical University, Wenzhou, Zhejiang, China.

[2]Department of Medicine, [10]Department of Pathology, Stony Brook University, Stony Brook, NY, 11794, USA

[3]Department of Gastrointestinal Medical Oncology, [5]Department of Cancer Biology, [6]Department of Experimental Therapeutics, University of Texas, MD Anderson Cancer Center, Houston, TX, 77030, USA

[4]Sun Yat-Sen University Cancer Center, State Key Laboratory of Oncology in South China, Collaborative Innovation Center for Cancer Medicine, Guangzhou, 510060, China.

[7]Cold Spring Harbor Laboratory, Cold Spring Harbor, NY, 11724, USA

[8]Departments of Pediatrics, Oncology, and Physiology and Pharmacology, Schulich School of Medicine, University of Western Ontario Children's Health Research Institute, London, ON, Canana N5C 2V5

This is the author's manuscript of the article published in final edited form as:

Luo, Y., Yang, Y., Liu, M., Wang, D., Wang, F., Bi, Y., … Lu, W. (2019). Oncogenic KRAS Reduces Expression of FGF21 in Acinar Cells to Promote Pancreatic Tumorigenesis in Mice on a High-Fat Diet. Gastroenterology. https://doi.org/10.1053/j.gastro.2019.07.030

[9]Department of Medical and Molecular Genetics, Indiana University School of Medicine. Indianapolis, IN, USA

[11]Department of Biochemistry and Molecular Biology, Mayo Clinic, Jacksonville, FL, USA

[12]Department of Gastroenterology, Changhai Hospital, Shanghai, China

[13]Division of Medical Oncology, Department of Medicine, Duke Cancer Institute, Duke University, Durham, NC, 27710, USA

[*] Authors share co-first authorship

[§]Authors share co-senior authorship

Funding: This work was supported by grants from the Start-up Funds from the Department of Medicine at Stony Brook University (W.L.), Sheikh Ahmed Bin Zayed Al Nahyan Center for Pancreatic Cancer Research from the University of Texas MD Anderson Cancer Center (W.L.), Pilot Project Grant at Stony Brook University (W.L.), National Institutes of Health DK052067 (C.D.L.), the Lockton Foundation Endowment (C.D.L.), China Scholarship Council #201403170269 (M.L.), #201603170128 (D.W.), #201703170106 (Y.B.), #201506580014 (J.J.), and National Institutes of Health 5P20CA192994-02 (E.L.).

Abbreviations: ADM, acinar-to-ductal metaplasia; CCL17, C-C chemokine ligand 17; CCL21a, C-C chemokine ligand 21A; CD3, cluster of differentiation 3; CD11b, macrophage cluster of differentiation 11; CD40L, Cluster of differentiation 40 ligand; CD68, cluster of differentiation 68; CK19, cytokeratin-19; COX2, cyclooxygenase-2; CXCL5, C-X-C motif chemokine ligand 5; CXCL9, C-X-C motif chemokine ligand 9; F4/80, EGF-like module-containing mucin-like hormone receptor-like 1; FGF, fibroblast growth factor; FGFR, fibroblast growth factor receptor; CSF2 (GM-CSF), granulocyte-macrophage colony-stimulating factor; HFD, high-fat diet; HPDE, human pancreatic ductal epithelial cells; IFNG, interferon gamma; IL21, interleukin 21; Ki-67, proliferation-related Ki-67 antigen; KLB, Klotho beta; KRAS, Kirsten rat sarcoma-2 viral (v-Ki-

ras2) oncogene homolog; CCL2 (MCP1), Monocyte/macrophage chemoattractant protein 1; CCL4 (MIP1b), macrophage inflammatory protein 1 beta; MIST1, muscle, intestine and stomach expression 1; MUC5, mucin 5 subtypes A and C; PanIN, pancreatic intraepithelial neoplasia; PDAC, pancreatic ductal adenocarcinoma; PPARA, peroxisome proliferator-activated receptor alpha; PPARG, peroxisome proliferator-activated receptor gamma; RORA, retinoid-related orphan receptor alpha; TGFB1, transforming growth factor beta; TNF, tumor necrosis factor alpha; TNFRSF11b, TNF receptor superfamily member 11b; UCP1, uncoupling protein 1.

Reprint requests

Weiqin Lu, Ph.D, E-mail: weiqin.lu@stonybrookmedicine.edu

Yongde Luo, Ph.D, E-mail: yongdeluo08@gmail.com

Conflicts of interest: The authors declare no potential conflicts of interest.

Author Contributions

W.L. conceived, designed, and supervised the whole project, and prepared the manuscript; C.D.L., J.L.A., and V.W.Y. provided the research platform, supervised the project, and prepared the manuscript. Y.Luo, Y.Y., and M.L. performed the experiments and drafted the manuscript. Y. Luo also conceived and designed the experiments, and contributed reagents. D.W., Y.B., J.J., S.L., Y. Liu., S.X., A.K.S., G.W., and C.K.L. performed immunohistochemistry analyses, qRT-PCR, Western blot analyses, data quantification, and assisted in breeding and genotyping the mice. D.W. and Y.B. performed acinar cell extraction and 3D explant cultures, F.W., R.C., X.W., A.B.B., H.H., G.L., C.L.P., X.L., B.J., R.A.W., W.P., Z.L., E.L., X. Li., T.J., and S.B. contributed the research materials, reagents, analysis tools, and discussion. M.W., K.R.S., Y.Y., and S.L. analyzed H&E images. All authors read and critically reviewed the manuscript.

Acknowledgements

We would like to express our gratitude to Dr. David A. Tuveson (Cold Spring Harbor Laboratory, NY) and Dr. Anirban Maitra (MD Anderson Cancer Center, TX) for providing insight and expertise that greatly improved the manuscript.

ACCEPTED MANUSCRIPT

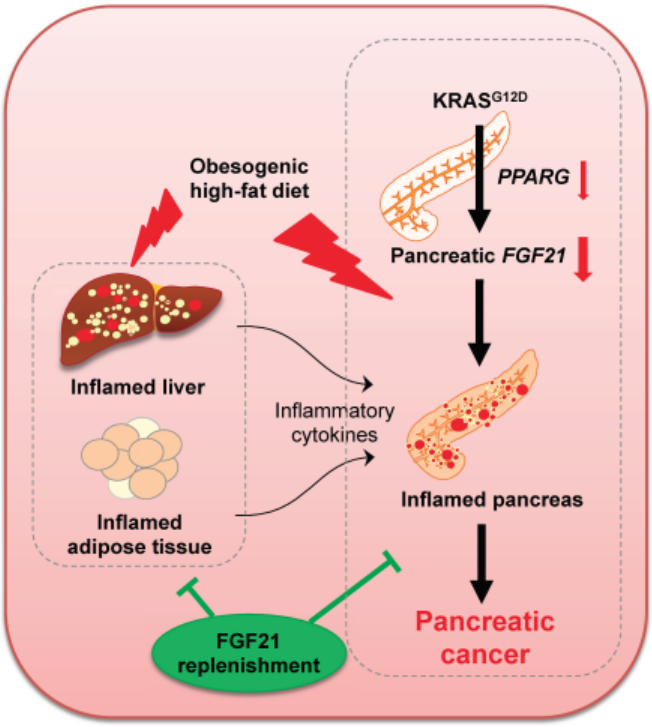
KRAS^{G12D}
PPARG
Pancreatic FGF21
Obesogenic high-fat diet
Inflamed liver
Inflammatory cytokines
Inflamed adipose tissue
Inflamed pancreas
FGF21 replenishment
Pancreatic cancer

ACCEPTED

ABSTRACT

Background & Aims: Obesity is a risk factor for pancreatic cancer. In mice, a high-fat diet (HFD) and expression of oncogenic KRAS lead to development of invasive pancreatic ductal adenocarcinoma (PDAC) by unknown mechanisms. We investigated how oncogenic KRAS regulates the expression of fibroblast growth factor 21 (FGF21), a metabolic regulator that prevents obesity, and the effects of recombinant human FGF21 (rhFGF21) on pancreatic tumorigenesis.

Methods: We performed immunohistochemical analyses of FGF21 levels in human pancreatic tissue arrays, comprising 59 PDAC specimens and 45 non-tumor tissues. We also studied mice with tamoxifen-inducible expression of oncogenic KRAS in acinar cells (*Kras*$^{G12D/+}$ mice) and *fElas*^{CreERT} mice (controls). *Kras*$^{G12D/+}$ mice were placed on a HFD or regular chow diet (control) and given injections of rhFGF21 or vehicle; pancreata were collected and analyzed by histology, immunoblots, quantitative PCR, and immunohistochemistry. We measured markers of inflammation in the pancreas, liver, and adipose tissue. Activity of RAS was measured based on the amount of bound GTP.

Results: Pancreatic tissues of mice expressed high levels of FGF21 compared with liver. FGF21 and its receptor proteins were expressed by acinar cells. Acinar cells that expressed *Kras*$^{G12D/+}$ had significantly lower expression of *Fgf21* mRNA, compared with acinar cells from control mice, partly due to downregulation of PPARG expression—a transcription factor that activates *Fgf21* transcription. Pancreata from *Kras*$^{G12D/+}$ mice on a control diet and given injections of rhFGF21 had reduced pancreatic inflammation, infiltration by immune cells, and acinar-to-ductal metaplasia compared with mice given injections of vehicle. HFD-fed *Kras*$^{G12D/+}$

mice given injections of vehicle accumulated abdominal fat, developed extensive inflammation, pancreatic cysts, and high-grade pancreatic intraepithelial neoplasias (PanINs); half the mice developed PDAC with liver metastases. HFD-fed *Kras*$^{G12D/+}$ mice given injections of rhFGF21 had reduced accumulation of abdominal fat and pancreatic triglycerides, fewer pancreatic cysts, reduced systemic and pancreatic markers of inflammation, fewer PanINs, and longer survival—only about 12% of mice developed PDACs and none of the mice had metastases. Pancreata from HFD-fed *Kras*$^{G12D/+}$ mice given injections of rhFGF21 had lower levels of active RAS than from mice given vehicle.

Conclusions: Normal acinar cells from mice and humans express high levels of FGF21. In mice, acinar expression of oncogenic KRAS significantly reduces FGF21 expression. When these mice are placed on a HFD, they develop extensive inflammation, pancreatic cysts, PanINs, and PDACs, which are reduced by injection of FGF21. FGF21 also reduces the GTP binding capacity of RAS. FGF21 might be used in prevention or treatment of pancreatic cancer.

Keywords: gene regulation, FGFR1, KLB, signaling

ACCEPTED MANUSCRIPT

Introduction

Pancreatic cancer is a fatal disease and is predicted to become the second leading cause of cancer-related deaths within a decade[1]. It is widely observed that mutations of *KRAS* (e.g., *KRAS*^{G12D}) are an essential initiating event for pancreatic cancer[2]. Previous studies have shown that mutant *Kras,* when expressed in pancreatic progenitor cells from the embryonic stage, is sufficient to drive PDAC in the *Pdx-1*^{Cre};*Kras*$^{LSL\text{-}G12D/+}$ (KC) mice[3]. However, human PDAC likely originates from somatic mutations in *KRAS* in acinar cells during adulthood, suggesting that mice expressing mutant *KRAS* in acinar cells after birth may be more clinically relevant. Notably, mutant *Kras* expressed at an endogenous level in adult acinar cells does not, on its own, lead to PDAC[4, 5], suggesting that an additional challenge is required.

Obesity is a modifiable risk factor for PDAC, and HFD is a major dietary component that drives obesity. Recent studies have shown that when fed a HFD, mice expressing an endogenous level of *Kras*$^{G12D/+}$ in acinar cells developed marked inflammation, PanIN lesions, and invasive PDAC leading to lethality with high penetrance[6]. However, the mechanism underlying the cooperation between HFD and oncogenic KRAS remains a major knowledge gap.

The endocrine FGF21 has emerged as a novel metabolic regulator for the maintenance of lipid, glucose, and energy homeostasis[7, 8]. Studies have shown that the liver is one of the major sources of endocrine FGF21 under stress conditions[9-11]. By serving as an endocrine factor, FGF21 promotes the clearance of systemic lipids and glucose, while enhancing insulin sensitivity, fatty acid oxidation, and energy expenditure without apparent effects on cell proliferation and growth[7, 12]. Therefore, FGF21 has the pharmacological potential to treat obesity, diabetes, and meta-inflammation[7, 12-14]. The effects of endocrine FGF21 are mediated

by binding to the transmembrane binary complex of fibroblast growth factors receptor 1 (FGFR1) and β-Klotho (KLB)[15-17]. In the pancreas, under wild-type KRAS conditions, FGF21 acts directly on acinar cells to protect the pancreas from pancreatitis and proteotoxic stress[18, 19]; however, the interaction between pancreatic FGF21 and oncogenic KRAS in pancreatic tumorigenesis has not been previously shown.

In the current study, by using mice with conditional knock-in of *Kras*$^{LSL\text{-}G12D/+}$ under the control of a TM-inducible *fElas*^{CreERT} driver as described[6, 20, 21], we report that FGF21, its target receptor FGFR1, and its co-receptor KLB were abundantly expressed in normal acinar cells, suggesting that acinar cells are both a source and a target of FGF21. The expression of pancreatic *FGF21* was dramatically downregulated, partly through a PPARG-dependent mechanism, upon an endogenous level of *Kras*$^{G12D/+}$ expression. Remarkably, under chronic HFD challenge, administration of rhFGF21, which compensates for the loss of FGF21 in acinar cells, significantly suppressed both pancreatic and systemic inflammation, inhibited RAS activation, PanIN lesions, tumor incidence, and liver metastasis, as well as extended the survival of *Kras*$^{G12D/+}$ mice in comparison to those without rhFGF21 treatment. Our results reveal that pancreatic FGF21 is downregulated by KRAS^{G12D}, which renders the pancreas vulnerable to obesogenic HFD challenge, leading to exacerbated inflammation and invasive PDAC, while pharmacological FGF21 counteracts the damaging effects of HFD and mitigates this vulnerability.

ACCEPTED MANUSCRIPT

Materials and Methods

Mouse strains

CreERT-LoxP recombination approaches were used to control gene expression in pancreatic acinar cells. *Kras*$^{LSL\text{-}G12D/+}$ mice, which possess the conditional knock-in of mutant *Kras*^{G12D}, were obtained as described[6]. *fElas*^{CreERT} mice, which express TM-regulated Cre recombinase under a full-length *Elastase* promoter specifically in acinar cells, were described previously[22]. *Kras*$^{LSL\text{-}G12D/+}$ mice and *fElas*^{CreERT} mice were cross-bred to generate *fElas*^{CreERT};*Kras*$^{LSL\text{-}G12D/+}$ double-transgenic mice (called *Kras*$^{G12D/+}$ after TM)[6, 23]. Alternatively, *Ptf1a*^{CreERT} mice[24] were crossed with *Kras*$^{LSL\text{-}G12D/+}$ mice to generate *Ptf1a*^{CreERT};*Kras*$^{LSL\text{-}G12D/+}$ mice (called *Ptf1a*^{CreERT};*Kras*$^{G12D/+}$ after TM)[25]. *Trp53*$^{LSL\text{-}R172H}$ mice[26] were crossed with *fElas*^{CreERT} mice to generate *fElas*^{CreERT};*Trp53*$^{LSL\text{-}R172H/+}$ (called *Trp53*$^{R172H/+}$ after TM) mice. All animal experiments were reviewed and approved by Stony Brook University Institutional IACUC and the University of Texas, MD Anderson Cancer Center IACUC.

Additional experimental details are provided in the Supplementary Information.

ACCEPTED MANUSCRIPT

Results

Pancreatic acinar cells are both a potential source and a target of FGF21

Previous studies have shown that HFD and $KRAS^{G12D}$ cooperate to promote PDAC with high penetrance[6], suggesting that acinar cells containing mutant KRAS are susceptible to chronic HFD challenge. FGF21 is an important regulator of lipid metabolism and elicits anti-obesity effects[8, 12] while also protecting the pancreas from pancreatitis and metabolic stress[18, 19]. In order to understand the role of FGF21 in the pancreas and pancreatic tumorigenesis, we employed the established *fElas*^{CreERT} and *fElas*^{CreERT};*Kras*$^{LSL\text{-}G12D/+}$ mice[6, 23]. We first compared the pancreatic and hepatic *Fgf21* expression in young adult *fElas*^{CreERT} control mice one week post-TM. Pancreatic *Fgf21* expression was significantly higher (>80 times) than that of hepatic tissue, which is known as the primary source of endocrine FGF21 under stress conditions (**Figure 1A**). This result concurs with a previous report showing that *Fgf21* is highly expressed in the normal pancreas[27]. Immunohistochemistry (IHC) and Western blot further confirmed the presence of FGF21 in acinar cells (**Figure 1B-C**). Correspondingly, the expression of pancreatic FGF21 receptor, *Fgfr1*, was significantly higher (>10 times) than that of the liver (**Figure 1D-E**). The expression of FGF21 co-receptor, *Klb*, was comparable to that of the liver (**Figure 1F**), which is known to express a high level of *Klb*[28, 29]. Western blot (**Figure 1G**) and IHC (**Figure 1H,** open arrow) studies further confirmed the abundant presence of KLB in acinar cells. Comparison of *Fgf21, Fgfr1,* and *Klb* expression across the liver, pancreas, and adipose tissues in 7-month-old *fElas*^{CreERT} mice after five months of TM induction revealed that pancreatic *Fgf21* expression remained the highest (**Figure 1I**). Both the pancreas and adipose tissue expressed significantly higher levels of *Fgfr1* than the liver (**Figure 1J**). *Klb* expression levels were comparable across all tissues (**Figure 1K**). Pancreatic *Fgf21* expression was stable regardless of the age and the duration post TM treatment (**Supplementary Figure 1A**). All these data

reveal that FGF21, FGFR1, and KLB are highly expressed in normal acinar cells, suggesting that pancreatic acinar cells are both a source and a target of FGF21.

FGF21 is a downstream target of oncogenic KRAS^{G12D}

To test if FGF21 plays a role in human pancreatic cancer, we performed IHC analysis of FGF21 in human pancreatic tissue arrays and found that the PDAC specimens (n=59) had substantially lower levels of FGF21 than normal human pancreatic tissues (n=45), which exhibited strong FGF21 positive staining in acinar cells (**Figure 2A-B**). FGF21 was also stained positively in normal ducts of both the normal human pancreas and PDAC specimens **(Supplementary Figure 2A, *inset***). In addition, from the human GEO database (https://www.ncbi.nlm.nih.gov/geoprofiles/78912317), *FGF21* expression in human PDAC tissues dropped significantly in comparison to the paired normal pancreata (n=39 pairs) (**Figure 2C**). Furthermore, *FGF21* expression in human pancreatic cancer cell lines carrying *KRAS* mutations decreased significantly in comparison to that of normal human pancreatic ductal epithelial (HPDE) cells (**Figure 2D**), suggesting an inverse association between pancreatic FGF21 and oncogenic KRAS.

Given that PDAC likely originates from acinar cells with somatic mutations in *KRAS* occurring after birth, we next analyzed the potential changes of FGF21 in the *fElas^{CreERT};Kras$^{LSL\text{-}G12D/+}$* mice that express an endogenous level of *Kras$^{G12D/+}$* in nearly 100% acinar cells upon TM induction[6]. A striking decrease of >100 fold in *Fgf21* expression was observed in mice five months post-TM relative to the age-matched *fElas^{CreERT}* mice (**Figure 2E**). IHC analysis confirmed the substantially lower levels of FGF21 in the pancreatic tissues of *Kras$^{G12D/+}$* mice compared to that of *fElas^{CreERT}* mice (**Supplementary Figure 2B**). To determine whether the drastic reduction of pancreatic *Fgf21* is an early event related to *Kras$^{G12D/+}$* expression, we first compared *Fgf21* expression in the 40-day-old *fElas^{CreERT}* control mice one week post-TM to that

without TM. No significant differences were observed between the two groups, suggesting that neither TM nor Cre recombinase affected *Fgf21* expression (**Supplementary Figure 2C**). We then compared *Fgf21* expression one week post-TM induction of $Kras^{G12D/+}$ to that of the age-matched (40 days old) mice without TM and found that *Fgf21* expression was significantly reduced upon $Kras^{G12D/+}$ induction (**Figure 2F**), suggesting that the downregulation of *Fgf21* is specific to $Kras^{G12D/+}$. Notably, this occurred when no obvious alterations of pancreatic histology were observed (**Figure 2G**).

To further confirm our observation that $KRAS^{G12D}$ specifically downregulates *Fgf21* expression, we employed another mouse strain, the $Ptf1a^{CreERT;}Kras^{LSL\text{-}G12D/+}$ mice[25]. qRT-PCR data showed that *Fgf21* expression was significantly reduced in these mice two weeks post-TM in comparison to the age-matched (two months of age) mice without TM induction (**Figure 2H**). No changes to the pancreatic histology were observed in the TM-induction group (**Supplementary Figure 2D**). Consistent with a role in tumorigenesis, the p53 mutations occur in 50–75% of human PDAC following an initiating mutation in *KRAS*. To determine if mutant p53 could also inhibit pancreatic *Fgf21*, we employed the $fElas^{CreERT;}Trp53^{LSL\text{-}R172H/+}$ mouse strain. Five months post-TM, no significant differences in pancreatic *Fgf21* expression were observed between the age-matched $Trp53^{R172H/+}$ and $fElas^{CreERT}$ mice (**Supplementary Figure 2E**), indicating that $Kras^{G12D/+}$, but not $Trp53^{R172H/+}$, specifically induces the marked downregulation of *Fgf21*. Furthermore, we compared *Fgfr1* and *Klb* expression in the age-matched $fElas^{CreERT}$ and $Kras^{G12D/+}$ mice one week post-TM. No significant changes for both genes were noticed (**Supplementary Figure 2F-G**).

Oncogenic KRAS reduces pancreatic *Fgf21* expression partially through downregulating *Pparg*

To understand how oncogenic KRAS may potentially intervene to suppress *FGF21* expression, we analyzed the expression of the transcription factors that are known to possess consensus binding sites on the *Fgf21* promoter region and responsible for *Fgf21* expression[9, 10, 30-32]. Among them, peroxisome proliferator-activated receptor gamma (*Pparg,* which encodes PPAR-gamma or PPARG), peroxisome proliferator-activated receptor alpha (*Ppara*), and retinoic acid receptor-related orphan receptor (*Rora*) were significantly downregulated (**Figure 2I, Supplementary Figure 2H-I**) in the same pancreatic tissues where *Fgf21* was reduced by $Kras^{G12D}$. However, other known *Fgf21*-regulating factors, such as *Rarb* and *ChREBP* (**Supplementary Figure 2J-K**), as well as *SREBP1* and *Lxrb* (data not shown), were not changed. Treatment of mutant *KRAS*-bearing Panc-1 cells that have a weak *FGF21* expression with a specific PPARG agonist, Rosiglitazone, resulted in a dose-dependent increase in *FGF21* expression (**Figure 2J**), suggesting that PPARG is a potential mediator of $KRAS^{G12D}$-downregulated expression of pancreatic *FGF21*.

Replenishment of FGF21 inhibits $KRAS^{G12D}$-mediated pancreatic inflammation and PanIN lesions under normal dietary conditions

Studies have demonstrated that under wild-type KRAS conditions, FGF21 signaling was induced in acinar cells upon experimental induction of pancreatitis and that genetic deletion of *Fgf21* exacerbated pancreatic injury[19]. FGF21 acts directly on acinar cells to promote exocrine secretion without increasing protein synthesis, thereby mitigating proteotoxic stress[18], suggesting that acinar cell FGF21 alleviates metabolic stress and associated pathogenic effects in the presence of wild-type KRAS. By contrast, our above data reveal that oncogenic KRAS downregulates acinar cell FGF21.

To determine if FGF21 replenishment plays a role in restricting $Kras^{G12D/+}$-mediated pancreatic inflammation and fibrosis under the normal diet (ND) conditions, we administered rhFGF21 to

Kras$^{G12D/+}$ mice for 10 weeks to compensate for the loss of acinar cell FGF21 (**Figure 3A**). rhFGF21 treatment significantly inhibited pancreatic inflammation and immune cell infiltration as measured by IHC staining of inducible cyclooxygenase-2 (COX-2) and F4/80, respectively, compared to those without rhFGF21 treatment (n=8) (**Figure 3B, Supplementary Figure 3A-B**). rhFGF21 also significantly reduced pancreatic fibrosis as measured by Sirius Red staining of collagen fibrils (**Figure 3B, Supplementary Figure 3C**). These data suggest that rhFGF21 supplementation effectively inhibits pancreatic inflammation and fibrosis induced by KRAS^{G12D} under the ND conditions.

To test whether rhFGF21 administration could inhibit KRAS^{G12D}-mediated acinar-to-ductal metaplasia (ADM), we evaluated acinar and duct cell markers in the ND-fed *Kras*$^{G12D/+}$ mice upon rhFGF21 treatment. Co-immunofluorescence (Co-IF) analyses of amylase and CK19, which mark acinar and duct cells, respectively, revealed that rhFGF21 treatment significantly reduced CK19+ staining and preserved amylase+ acinar cells compared to those without rhFGF21 treatment (**Figure 3C-E**). These data suggest that rhFGF21 suppresses the ADM reprogramming induced by oncogenic KRAS under normal feeding conditions.

To determine whether rhFGF21 directly acts on acinar cells, we isolated acinar cell clusters from 80-day-old *Kras*$^{G12D/+}$ mice one week post-TM and seeded them in collagen plates for 3-dimensional (3D) explant cultures with daily rhFGF21 treatment. On day one, treatment with rhFGF21 had little effects on the acinar cell clusters; however, by day four, rhFGF21 significantly inhibited ductal cell formation compared to PBS treatment group (**Figure 3F, Supplementary Figure 3D**), suggesting that rhFGF21 directly acts on acinar cells to inhibit KRAS^{G12D}-mediated ADM reprogramming.

As ADM is regarded as the precursor to the development of PanIN lesions, we evaluated the effects of FGF21 administration on $KRAS^{G12D}$-mediated PanIN lesions using Alcian blue staining for acidic mucins and IHC staining for Mucin 5AC (MUC5). rhFGF21 injections caused a noticeable reduction in both acidic mucins and MUC5 compared to those without FGF21 treatment (**Figure 3G, Supplementary Figure 3E-F**). Using IHC analysis, we observed that rhFGF21 suppressed ductal cell proliferation as measured by the decreased levels of Ki-67 and cyclin D1 (**Figure 3H-J**). Altogether, our data indicate that the exogenous supplementation of FGF21 to *Kras*$^{G12D/+}$ mice that have a dramatic reduction of FGF21 in acinar cells results in significant beneficial effects on the inhibition of pancreatic inflammation, ADM, and PanIN lesions under the ND conditions.

Pharmacological administration of FGF21 inhibits HFD and $KRAS^{G12D}$ induced PanIN lesions and PDAC

Inspired by the above data, we proceeded to determine if FGF21 plays a suppressive role in HFD and KRAS mediated invasive PDAC by treating the *Kras*$^{G12D/+}$ mice concurrently with HFD and rhFGF21 for 10 weeks (**Figure 4A**). The HFD-fed *Kras*$^{G12D/+}$ mice accumulated abdominal fat and developed multiple pancreatic cysts (**Figure 4B**). In contrast, treatment with rhFGF21 alleviated abdominal fat accumulation and pancreatic cysts (**Figure 4B**). Consistently, rhFGF21 administration reduced the accumulation of pancreatic triglycerides in comparison to those without rhFGF21 treatment (**Supplementary Figure 4A**). Histological analysis revealed that the HFD-fed *Kras*$^{G12D/+}$ mice displayed high-grade PanIN lesions and PDAC with 50% penetrance (**Figure 4C**). In marked contrast, with rhFGF21 treatment, most of the mice (87.5%) exhibited well-preserved parenchyma and acinar cell content with only early stage PanIN lesions (**Figure 4C-D**). Only one out of eight mice treated with rhFGF21 developed PDAC.

Assessment of damage to pancreatic tissues revealed that chronic HFD consumption led to a significant decrease of amylase, which marks acinar cell content, while rhFGF21 treatment restored the lost amylase content (**Figure 4E, Supplementary Figure 4B)**. Alpha-smooth muscle actin (α-SMA), which marks the levels of pancreatic stellate cell activation, was strongly elevated in the HFD-fed *Kras*$^{G12D/+}$ mice. However, this elevation was significantly suppressed by chronic treatment with rhFGF21 (**Figure 4E**, **Supplementary Figure 4C**). The Co-IF analysis further revealed that rhFGF21 greatly reduced CK19+ staining and preserved acinar cells (amylase+) compared to the HFD-fed *Kras*$^{G12D/+}$ mice without rhFGF21 treatment (**Figure 4F**, **Supplementary Figure 4D-E**). A similar pattern to that observed for amylase was found for MIST1, a transcription factor essential for maintaining an adult acinar cell phenotype (**Figure 4F**, **Supplementary Figure 4F**). These data suggest that rhFGF21 preserved acinar cells and inhibited stromal activation induced by HFD in *Kras*$^{G12D/+}$ mice. Furthermore, we observed prominent positive stains of acidic mucins and MUC5 in the pancreata of the HFD-fed *Kras*$^{G12D/+}$ mice; however, rhFGF21 treatment significantly inhibited these PanIN markers (**Figure 4G, Supplementary Figure 4G-H**). Our data suggest that the replenishment of FGF21 suppresses HFD and KRAS^{G12D} induced rapid PanIN lesions and PDAC.

To determine whether the significant downregulation of pancreatic FGF21 by KRAS^{G12D} can lead to a reduction of serum FGF21 levels, which may induce systemic metabolic alterations, we measured serum FGF21 levels pre-TM, one week and 10 weeks post-TM induction of *Kras*$^{G12D/+}$. No significant differences in serum FGF21 levels were observed (**Supplementary Figure 4I-J**), indicating that alteration of pancreatic FGF21 by KRAS^{G12D} does not influence circulating FGF21 levels.

Pharmacological FGF21 inhibits HFD and KRAS^{G12D} induced pancreatic inflammation

Chronic HFD causes inflammation, which cooperates with oncogenic KRAS to drive PDAC[4]. To understand whether the tumor-suppressive effect of rhFGF21 is through alleviation of pancreatic inflammation, we analyzed the protein expression of COX-2, which was up-regulated in the HFD-fed *Kras*$^{G12D/+}$ mice[6]. Indeed, these mice exhibited intense focal staining of COX-2 along the pancreatic ducts; however, rhFGF21 treatment significantly decreased COX-2+ staining to levels comparable to the ND-fed *Kras*$^{G12D/+}$ mice (**Figure 5A**, **Supplementary Figure 5A**). Furthermore, macrophages, as detected by F4/80+ staining, were abundant in the pancreata of the HFD-fed *Kras*$^{G12D/+}$ mice; however, rhFGF21 significantly inhibited HFD-induced macrophage infiltration (**Figure 5A**, **Supplementary Figure 5B**). In a similar manner, CD3, as a marker of peripheral T cell infiltration, was significantly elevated under chronic HFD insult, while rhFGF21 alleviated T cell infiltration (**Figure 5A**, **Supplementary Figure 5C**). Analysis of extracellular matrix collagen deposition that marks pancreatic fibrosis revealed that although the ND-fed *fElas*^{CreERT} mice displayed a minimal collagen staining that was primarily localized around the blood vessels and the peri-lobular spaces, the HFD-fed *Kras*$^{G12D/+}$ mice exhibited intense collagen deposition surrounding the neoplastic ductal structures, indicating a robust fibrotic response. In contrast, FGF21 supplementation significantly reduced collagen levels (**Figures 5A**, **Supplementary Figure 5D**).

To better understand the suppressive role of FGF21 in pancreatic inflammation promoted by the cooperative interaction between HFD and KRAS^{G12D}, we analyzed the expression of an array of inflammation-associated cytokines/chemokines and receptors comparatively by qRT-PCR. Of note, the pancreata of the ND-fed *Kras*$^{G12D/+}$ mice showed significant increases in the expression of *Cxcl5*, *Tgfb1, Ccl2, Csf2, Tnf,* and *Tnfrsf11b* in comparison to those of the ND-fed *fElas*^{CreERT} mice, suggesting that pancreatic inflammation is mediated by oncogenic KRAS in this context (**Figure 5B-C, Supplementary Figure 5E-H**). HFD treatment further enhanced the expression of these genes (**Figure 5B-C, Supplementary Figure 5E-H**), indicating a significant

inflammatory effect of obesogenic HFD on the pancreas. Interestingly, although pancreatic *Ccl17* was not affected by KRAS^{G12D} under the ND conditions, it was markedly upregulated in response to the HFD challenge in the *Kras*$^{G12D/+}$ mice (**Supplementary Figure 5I**). Importantly, rhFGF21 administration significantly suppressed the augmented expression of all these genes (**Figure 5B-C, Supplementary Figure 5E-I**). These data suggest a prominent anti-inflammatory role of FGF21 in the pancreas. On the other hand, the expression levels of the cytokines that have anti-inflammation or anti-neoplastic functions, including *Ccl19, Ifng, Il21, Cd40l, Ccl21a,* and *Cxcl9*, were significantly downregulated in the HFD-fed *Kras*$^{G12D/+}$ mice, while administration of rhFGF21 effectively restored their expression (**Supplementary Figure 5J-O**).

We have previously shown that RAS activity is an important determinant in pancreatic tumorigenesis, and that inflammation enhances RAS activity[21, 33]. As pharmacological rhFGF21 significantly suppressed HFD-promoted pancreatic inflammation, we tested if this would lead to a reduction of RAS activity in the pancreata of the HFD-fed *Kras*$^{G12D/+}$ mice. Indeed, we observed that the HFD-enhanced RAS hyperactivity was significantly inhibited by rhFGF21 (**Figure 5D, Supplementary Figure 5P**). These data indicate that the beneficial effects of FGF21 in protecting the pancreas from neoplastic progression are attributable to the inhibition of the accentuated inflammation and RAS hyperactivation induced by HFD.

Correspondingly, rhFGF21 treatment significantly reduced cyclin D1 and Ki-67 levels in the pancreatic ductal cells of the HFD-fed *Kras*$^{G12D/+}$ mice compared to those without rhFGF21 treatment (**Figure 5E**, **Supplementary Figure 5Q-R**). These data indicate that the supplementation of rhFGF21 to compensate for the loss of pancreatic FGF21 inhibits pancreatic tumor cell proliferation induced by the synergistic cooperation between KRAS^{G12D} and HFD.

Pharmacological FGF21 inhibits HFD-induced liver and adipose tissue inflammation

As chronic HFD imposes adverse metabolic effects on adipose tissue and the liver, which are among the direct or indirect targets of endocrine FGF21[9, 10, 16], we therefore tested the anti-inflammatory effects of rhFGF21 on both tissues. The ND-fed *Kras*$^{G12D/+}$ mice showed no significant differences in the inflammation markers compared to the ND-fed *fElas*^{CreERT} mice in either the liver or the adipose tissue (**Figure 6A-I**, **Supplementary Figure 6A-B**), suggesting that the liver and adipose tissue do not impose significant inflammatory stress on the pancreas under the ND conditions, and therefore, the observed pancreatic inflammation and associated pathologies in **Figure 3** are attributable to KRAS^{G12D} in this context. Thus, FGF21 plays a direct role in restricting KRAS^{G12D}-mediated pancreatic inflammation and associated pathogenesis.

Furthermore, chronic HFD significantly elevated the expression of *Ccl2*, *Ccl4, CD68,* and *CD11b* in both the liver and adipose tissues, as well as adipose *Tgfb1, Tnf*, and *Ccl11*, while rhFGF21 effectively suppressed these inflammation markers (**Figure 6A-I**, **Supplementary Figure 6A-B**). As a metabolic marker of adipose tissue response, adipose *Ucp1* underwent a striking increase of >40 fold with rhFGF21 treatment (**Supplementary Figure 6C**). Furthermore, the anti-inflammatory and anti-fibrotic adipokine, *Adipoq,* was also significantly elevated upon rhFGF21 treatment (**Supplementary Figure 6D**). These data suggest that rhFGF21 inhibits the HFD-induced systemic inflammation that otherwise may impinge on the pancreas through secretory cytokines or adipokines.

Pharmacological FGF21 inhibits HFD and KRAS^{G12D} induced liver metastasis and prolongs survival

Next, we determined whether pharmacological administration of rhFGF21 would prolong the overall survival and inhibit liver metastasis in the HFD-fed *Kras*$^{G12D/+}$ mice. We first observed that mice fed a HFD had a substantial increase in body weight; however, this was not evident under rhFGF21 treatment despite a continued HFD consumption (**Figure 7A**). Furthermore, the

survival rate of the HFD-fed *Kras*$^{G12D/+}$ mice significantly decreased compared to the age-matched ND-fed *Kras*$^{G12D/+}$ mice, with median survival rates of 229 days and 352 days, respectively. Treatment with rhFGF21 prolonged the median survival of the HFD-fed *Kras*$^{G12D/+}$ to 323 days (**Figure 7B**). *Kras*$^{G12D/+}$ mice fed a ND and concurrently treated with rhFGF21 showed a better survival rate than the ND-fed *Kras*$^{G12D/+}$ mice (**Figure 7B**), which do not spontaneously develop obesity. Regardless of the nature of the diets and the survival rates, the aged *Kras*$^{G12D/+}$ mice eventually developed PDAC (**Figure 7C**). The cancerous cells formed ductal structures (closed arrow), showing severe architectural and cytological atypia with frequent mitotic figures and abundant interstitial fibrosis (**Figure 7C**).

Over 50% of the HFD-fed *Kras*$^{G12D/+}$ mice progressed to liver metastasis. Multiple metastatic nodules with distinct borders were mostly found located on the liver surface in the HFD treatment group (**Figure 7D**, upper panel). Histological analyses revealed prominent metastatic foci on liver sections of the HFD treatment mice (**Figure 7D**, middle panel), and CK19 positive staining further confirmed the liver metastases in the HFD-fed *Kras*$^{G12D/+}$ mice. In contrast, the HFD-fed *Kras*$^{G12D/+}$ mice concurrently treated with rhFGF21 failed to develop liver metastases (**Figure 7D**, lower panel, **Supplementary Figure 7A**).

In summary, our studies show that KRAS^{G12D}, partly through downregulating *Pparg*, reduces *Fgf21*, which in turn creates a vulnerability to obesogenic HFD challenge, leading to extensive inflammation, RAS hyperactivation, PanIN lesions, and invasive PDAC. Pharmacological supplementation of FGF21 mitigates both pancreatic and systemic inflammation, resulting in the suppression of RAS hyperactivity and PDAC development (**Figure 7E**).

Discussion

Obesity dramatically increases the risk of pancreatic cancer, which remains one of the most aggressive malignancies[34], and the chronic consumption of a HFD is known as a primary dietary factor in promoting obesity. As the prevalence of obesity has been increasing at an alarming rate, obesity-associated pancreatic cancer poses an even greater threat. Thus, gaining a better understanding of HFD-promoted pancreatic cancer is urgent, as it will provide new insights into possible effective intervention strategies. Experimentally, HFD promotes oncogenic KRAS-mediated PDAC, indicating that mutations in KRAS render mice susceptible to obesogenic HFD insults leading to PDAC. However, the mechanism underlying such vulnerability is unclear. In this study, we made several novel observations concerning the roles of FGF21, metabolic regulator that prevents obesity, in the pancreas and oncogenic KRAS-mediated pancreatic tumorigenesis. First, we find that acinar cells express high levels of *Fgf21, Fgfr1*, and *Klb* under normal feeding conditions, suggesting that acinar cells are both a source and a target of FGF21. Second, we report for the first time that *Fgf21* expression in acinar cells is highly sensitive to mutant $KRAS^{G12D}$, showing remarkable decrease upon the expression of $Kras^{G12D/+}$ at an endogenous level when no overt alterations of pancreatic histology are noted. Third, we show that the significant downregulation of *Fgf21* by mutant $KRAS^{G12D}$ is partly mediated by the reduced PPARG. Fourth, we note that replenishment of the lost FGF21 directly inhibits pancreatic inflammation, transdifferentiation of acinar cells into ductal cells, and PanIN lesions under the ND conditions. Fifth, pharmacological FGF21 significantly mitigates inflammation in both the pancreas and systemic liver and adipose tissue under the HFD conditions. Sixth, FGF21 supplementation significantly inhibits HFD-promoted pancreatic RAS hyperactivity. Finally, pharmacological FGF21 significantly ameliorates pancreatic pathogenic responses, leading to the significant delay of PDAC development and extension of survival under obesogenic HFD challenge.

We have provided evidence to support that KRAS^{G12D} downregulates pancreatic *FGF21* expression. First, we show that PADC patient tissues and mutant *KRAS*-bearing pancreatic cancer cells exhibit a significant reduction of *FGF21* compared to their normal counterparts. Second, in several *Kras*$^{G12D/+}$ mouse strains with different Cre drivers, we show that KRAS^{G12D} significantly inhibits *Fgf21* expression. Third, we note that *Pparg*, *Ppara,* and *Rora*, which were shown to induce *FGF21* expression[9, 10, 30-32], are downregulated by KRAS^{G12D} expression. Finally, treatment of pancreatic cancer cells with PPARG agonist increased *FGF21* expression in a dose-dependent manner, suggesting a role of PPARG in regulating pancreatic *FGF21*. It would be interesting to investigate further the functional roles of PPARG, PPARA, and RORA in regulating pancreatic *FGF21* and pancreatic tumorigenesis.

Our results indicate a prominent role of FGF21 in directly protecting the pancreas from neoplastic progression induced by KRAS^{G12D}. First, we show that acinar cells express high levels of FGF21 and its receptor complex, indicating an autocrine/paracrine mode of FGF21 action in the pancreas, which aligns with previous findings showing that FGF21 directly targets acinar cells[18, 19]. Second, the pancreata of the ND-fed *Kras*$^{G12D/+}$ mice, which do not develop obesity and systemic inflammation, were effectively protected from KRAS^{G12D}-driven inflammation and neoplastic progression by rhFGF21, indicating a direct protective effect of FGF21 on the pancreas with minimal systemic influence. Third, we show that rhFGF21 directly inhibits ADM in the *in vitro* 3D explant cultures of acinar clusters, which is not subject to systemic metabolic influence.

Pancreatic function and systemic metabolism are inextricably linked. In the *Kras*$^{G12D/+}$ mice, chronic consumption of HFD leads to obesity and invasive PDAC, while rhFGF21 ameliorates these detrimental systemic and local pancreatic effects of HFD. We show that HFD induces

inflammation in both the pancreas and systemic liver and adipose tissue, while these adverse effects are effectively inhibited by rhFGF21, emphasizing the broad anti-inflammatory role of FGF21. Decreased inflammation was accompanied by the suppression of inflammation-associated fibrosis, PanIN lesions, and PDAC development. Importantly, we observed that the HFD-enhanced pancreatic RAS activity was also significantly reduced by rhFGF21. Furthermore, previous studies have shown that inhibition of local pancreatic inflammation through ablation of COX-2 in acinar cells markedly suppressed HFD and $KRAS^{G12D}$ mediated pancreatic neoplastic progression[6], supporting that the inhibition of local pancreatic inflammation is critical to the suppression of pancreatic tumorigenesis. Collectively, our data suggest that in addition to the noticeable systemic anti-inflammatory effects, the anti-inflammatory effects of rhFGF21 on the pancreas are essential to the suppression of HFD-promoted inflammatory damage and RAS hyperactivation, leading to the protection of the pancreas from neoplastic progression.

Previous studies focused on the pathophysiological roles of FGF21 in the liver and pancreas in the setting of wild-type KRAS[18, 19, 35], which showed that FGF21 exhibits a marked elevation in response to stress-inducing conditions, including the ingestion of a HFD[11]. Unlike these previous studies, however, our study shows that pancreatic FGF21 is negatively regulated by oncogenic KRAS. By abrogating FGF21, oncogenic KRAS allows the malevolent metabolic effect of chronic HFD consumption to take its maximal toll on the pancreas. In light of this fact, the loss of pancreatic FGF21 specifically by oncogenic KRAS is significant, as this breaks a stress-defensive barrier in the path towards PDAC development.

We observed multiple small pancreatic cysts in the HFD-fed $Kras^{G12D/+}$ mice; however, rhFGF21 treatment effectively inhibited this phenomenon, suggesting that inflammation is likely the cause of pancreatic cysts. In patients, mucinous cystic lesions are precursors to invasive pancreatic

cancer. Therefore, it is possible that FGF21 holds the potential to reverse mucinous pancreatic cysts and reduce the risk of pancreatic cancer in such patients.

In summary, our findings reveal a previously unknown critical vulnerability conferred by oncogenic KRAS, highlight pancreatic FGF21 as an important downstream target of oncogenic KRAS, and identify pharmacological FGF21 as a putative intervention strategy to hinder pancreatic inflammation and cancer development in the context of obesity.

ACCEPTED MANUSCRIPT

REFERENCE:

1. Rahib L, Smith BD, Aizenberg R, et al. Projecting cancer incidence and deaths to 2030: the unexpected burden of thyroid, liver, and pancreas cancers in the United States. Cancer Res 2014;74:2913-21.
2. Collins MA, Bednar F, Zhang Y, et al. Oncogenic Kras is required for both the initiation and maintenance of pancreatic cancer in mice. J Clin Invest 2012;122:639-53.
3. Hingorani SR, Petricoin EF, Maitra A, et al. Preinvasive and invasive ductal pancreatic cancer and its early detection in the mouse. Cancer Cell 2003;4:437-50.
4. Guerra C, Collado M, Navas C, et al. Pancreatitis-induced inflammation contributes to pancreatic cancer by inhibiting oncogene-induced senescence. Cancer Cell 2011;19:728-39.
5. Guerra C, Schuhmacher AJ, Canamero M, et al. Chronic pancreatitis is essential for induction of pancreatic ductal adenocarcinoma by K-Ras oncogenes in adult mice. Cancer Cell 2007;11:291-302.
6. Philip B, Roland CL, Daniluk J, et al. A high-fat diet activates oncogenic Kras and COX2 to induce development of pancreatic ductal adenocarcinoma in mice. Gastroenterology 2013;145:1449-58.
7. **Foltz IN, Hu S, King C,** et al. Treating diabetes and obesity with an FGF21-mimetic antibody activating the betaKlotho/FGFR1c receptor complex. Sci Transl Med 2012;4:162ra153.
8. Kharitonenkov A, Shiyanova TL, Koester A, et al. FGF-21 as a novel metabolic regulator. J Clin Invest 2005;115:1627-35.
9. Badman MK, Pissios P, Kennedy AR, et al. Hepatic fibroblast growth factor 21 is regulated by PPARalpha and is a key mediator of hepatic lipid metabolism in ketotic states. Cell Metab 2007;5:426-37.

10. Inagaki T, Dutchak P, Zhao G, et al. Endocrine regulation of the fasting response by PPARalpha-mediated induction of fibroblast growth factor 21. Cell Metab 2007;5:415-25.
11. Yang C, Lu W, Lin T, et al. Activation of Liver FGF21 in hepatocarcinogenesis and during hepatic stress. BMC Gastroenterol 2013;13:67.
12. Gaich G, Chien JY, Fu H, et al. The effects of LY2405319, an FGF21 analog, in obese human subjects with type 2 diabetes. Cell Metab 2013;18:333-40.
13. Talukdar S, Zhou Y, Li D, et al. A Long-Acting FGF21 Molecule, PF-05231023, Decreases Body Weight and Improves Lipid Profile in Non-human Primates and Type 2 Diabetic Subjects. Cell Metab 2016;23:427-40.
14. **Wu AL, Kolumam G,** Stawicki S, et al. Amelioration of type 2 diabetes by antibody-mediated activation of fibroblast growth factor receptor 1. Sci Transl Med 2011;3:113ra126.
15. Ogawa Y, Kurosu H, Yamamoto M, et al. BetaKlotho is required for metabolic activity of fibroblast growth factor 21. Proc Natl Acad Sci U S A 2007;104:7432-7.
16. **Adams AC, Yang C,** Coskun T, et al. The breadth of FGF21's metabolic actions are governed by FGFR1 in adipose tissue. Mol Metab 2012;2:31-7.
17. Yang C, Jin C, Li X, et al. Differential specificity of endocrine FGF19 and FGF21 to FGFR1 and FGFR4 in complex with KLB. PLoS One 2012;7:e33870.
18. **Coate KC, Hernandez G,** Thorne CA, et al. FGF21 Is an Exocrine Pancreas Secretagogue. Cell Metab 2017;25:472-80.
19. Johnson CL, Weston JY, Chadi SA, et al. Fibroblast Growth Factor 21 Reduces the Severity of Cerulein-Induced Pancreatitis in Mice. Gastroenterology 2009;137:1795-804
20. Huang H, Daniluk J, Liu Y, et al. Oncogenic K-Ras requires activation for enhanced activity. Oncogene 2014;33:532-5.
21. Daniluk J, Liu Y, Deng D, et al. An NF-kappaB pathway-mediated positive feedback loop amplifies Ras activity to pathological levels in mice. J Clin Invest 2012;122:1519-28.

22. Ji B, Song J, Tsou L, et al. Robust acinar cell transgene expression of CreErT via BAC recombineering. Genesis 2008;46:390-5.

23. **Wang D, Bi Y, Hu L, Luo Y,** et al. Obesogenic high-fat diet heightens aerobic glycolysis through hyperactivation of oncogenic KRAS. Cell Commun Signal 2019;17:19.

24. Pan FC, Bankaitis ED, Boyer D, et al. Spatiotemporal patterns of multipotentiality in Ptf1a-expressing cells during pancreas organogenesis and injury-induced facultative restoration. Development 2013;140:751-64.

25. He P, Yang JW, Yang VW, et al. Kruppel-like Factor 5, Increased in Pancreatic Ductal Adenocarcinoma, Promotes Proliferation, Acinar-to-Ductal Metaplasia, Pancreatic Intraepithelial Neoplasia, and Tumor Growth in Mice. Gastroenterology 2018;154:1494-1508 e13.

26. Hingorani SR, Wang L, Multani AS, et al. Trp53R172H and KrasG12D cooperate to promote chromosomal instability and widely metastatic pancreatic ductal adenocarcinoma in mice. Cancer Cell 2005;7:469-83.

27. Adams AC, Coskun T, Cheng CC, et al. Fibroblast growth factor 21 is not required for the antidiabetic actions of the thiazoladinediones. Mol Metab 2013;2:205-14.

28. Fon Tacer K, Bookout AL, Ding X, et al. Research resource: Comprehensive expression atlas of the fibroblast growth factor system in adult mouse. Mol Endocrinol 2010;24:2050-64.

29. Kurosu H, Choi M, Ogawa Y, et al. Tissue-specific expression of betaKlotho and fibroblast growth factor (FGF) receptor isoforms determines metabolic activity of FGF19 and FGF21. J Biol Chem 2007;282:26687-95.

30. Muise ES, Azzolina B, Kuo DW, et al. Adipose fibroblast growth factor 21 is up-regulated by peroxisome proliferator-activated receptor gamma and altered metabolic states. Mol Pharmacol 2008;74:403-12.

31. Wang H, Qiang L, Farmer SR. Identification of a domain within peroxisome proliferator-activated receptor gamma regulating expression of a group of genes containing fibroblast growth factor 21 that are selectively repressed by SIRT1 in adipocytes. Mol Cell Biol 2008;28:188-200.

32. Wang Y, Solt LA, Burris TP. Regulation of FGF21 expression and secretion by retinoic acid receptor-related orphan receptor alpha. J Biol Chem 2010;285:15668-73.

33. Ji B, Tsou L, Wang H, et al. Ras activity levels control the development of pancreatic diseases. Gastroenterology 2009;137:1072-82, 1082 e1-6.

34. Incio J, Liu H, Suboj P, et al. Obesity-Induced Inflammation and Desmoplasia Promote Pancreatic Cancer Progression and Resistance to Chemotherapy. Cancer Discov 2016;6:852-69.

35. Singhal G, Kumar G, Chan S, et al. Deficiency of fibroblast growth factor 21 (FGF21) promotes hepatocellular carcinoma (HCC) in mice on a long term obesogenic diet. Mol Metab 2018;13:56-66.

Author names in bold designate shared co-first authorship.

ACCEPTED MANUSCRIPT

FIGURE LEGENDS

Figure 1. Pancreatic acinar cells are both a source and a target of FGF21.

All mice in A-H were fed a ND, induced by TM at 70 days of age, and sacrificed one week post-TM. (A) qRT-PCR analysis of *Fgf21* expression in the liver (n=11) and pancreas (Panc, n=11) of *fElas*^{CreERT} mice. (B) IHC analysis of FGF21 on the liver and pancreas sections. 200x. (C) Western blot analysis for FGF21 levels. (D) Semi-quantitative RT-PCR analysis for *Fgfr1* in the liver (L) and pancreas (P). (E-F) qRT-PCR analysis for *Fgfr1* and *Klb* in the liver (n=9) and pancreas (n=9). (G) Western blot analysis for KLB in the pancreas (p). (H) IHC analysis of KLB in pancreatic sections. 200x. All mice in I-K were fed a ND, induced by TM at 70 days of age, and sacrificed at 7 months of age. Comparative qRT-PCR analysis for *Fgf21* (I), *Fgfr1* (J) and *Klb* (K) in the liver (n=7), pancreas (n=7), and adipose tissue (n=7) of *fElas*^{CreERT} mice. Open arrow, acinar cells. Closed arrow, islet cells. Data are means ± SEM. **, p*<0.05; **, *p*<0.01; ****, *p*<0.0001; ns, not significant.

Figure 2. KRAS^{G12D} downregulates *Fgf21* gene expression in acinar cells.

(A) IHC analysis for FGF21 levels in tissue arrays of human normal pancreas (n=45) and PDAC (n=59) (40x). *Inset:* 200x. (B) Quantitation of human FGF21 levels as described in 2A. (C) Human *FGF21* expression in 39 pairs of normal and tumor tissues resected from pancreatic cancer patients as collected in the GEO database (https://www.ncbi.nlm.nih.gov/geo/tools/profileGraph.cgi?ID=GDS4103:221433_at). (D) qRT-PCR analysis of *FGF21* in human pancreatic cancer cell lines carrying *KRAS* mutations. Human normal pancreatic ductal epithelial (HPDE) cells served as a control. All mice in E-I were fed a ND. (E) qRT-PCR analysis of pancreatic *Fgf21* in 7-month-old *Kras*$^{G12D/+}$ (n=11) or *fElas*^{CreERT} mice (n=5) mice five months post-TM. (F) qRT-PCR analysis of pancreatic *Fgf21* in 40-day-old *Kras*$^{G12D/+}$ mice one week post-TM (n=7) or without TM (n=9). (G) Representative histology of the pancreata as in 2F. 200x. (H) qRT-PCR analysis of pancreatic *Fgf21* of two-month-old

Ptf1a^{CreERT};*Kras*$^{G12D/+}$ mice two weeks post-TM (n=3) or without TM (n=3). (I) qRT-PCR analysis of pancreatic *Pparg* in 40-day-old *Kras*$^{G12D/+}$ mice one week post-TM (n=7) or without TM (n=9). (J) qRT-PCR analysis of *FGF21* in Panc-1 cells with Rosiglitazone treatment. Data are mean ± SD. *, p<0.05; **, p<0.01; ***, p<0.001; ****, p<0.0001.

Figure 3. Replenishment of FGF21 suppresses KRAS^{G12D}-induced pancreatic inflammation and PanIN lesions under ND conditions.

(A) Experimental scheme for B-E and G-J: 70-day-old ND-fed *Kras*$^{G12D/+}$;*fElas*^{CreERT} mice were treated with TM at 70 days of age to induce *Kras*$^{G12D/+}$ expression in acinar cells, and then treated with rhFGF21 (0.5 mg/kg body weight/day) (n=10) or PBS (n=8) for ten weeks. (B) IHC staining of COX-2 and F4/80, and Sirius Red staining of collagen on pancreatic sections of *Kras*$^{G12D/+}$ mice with indicated treatments. 200x. (C) Co-immunofluorescence (Co-IF) analysis of amylase and CK19 as indicated. 200x. (D-E) Quantitation of amylase+ areas or CK19+ areas on pancreatic sections (n=4) as described in 3C. (F) The explanted acinar cell 3D clusters isolated from 80-day-old *Kras*$^{G12D/+}$ mice one week post-TM were treated daily with rhFGF21 or PBS and then analyzed by brightfield images on day 1, H&E staining on day 4, and Co-IF staining of amylase and CK19 on day 4. (G) Alcian blue staining of acidic mucins and IHC staining of MUC5. (H) IHC analyses of Ki-67 (ND, n=4; ND+rhFGF21, n=4) and Cyclin D1 (ND, n=5; ND+rhFGF21, n=3). (I-J) Quantitation of Ki-67 and Cyclin D1 levels in 3H. Results were expressed as mean ± SD. **, p<0.01.

Figure 4. Supplementation of FGF21 suppresses HFD and KRAS^{G12D} induced PanIN lesions and PDAC.

(A) Experimental scheme: 70-day-old ND-fed *Kras*$^{G12D/+}$;*fElas*^{CreERT} mice were treated with TM to induce *Kras*$^{G12D/+}$ expression and randomly separated into ND, HFD, or HFD with rhFGF21

treatment groups (n=8 per group) for ten weeks. The age-matched ND-fed *fElas*^{CreERT} mice (n=8) served as controls. (B) Gross images of *Kras*$^{G12D/+}$ mice (left) and the pancreata (right) after the indicated treatments. Closed arrows, multiple pancreatic cysts. (C) Histology of representative pancreata. Closed arrows, PanIN lesions. Open arrows, cancerous ductal structure. 100x. (D) Average grades of PanIN1/2 and PanIN3 lesions as in 4C. F21, rhFGF21. (E) Western blot analysis of pancreatic amylase and α-SMA as indicated. (F) Co-IF analysis of pancreatic amylase and CK19 or IHC analysis of MIST1. 200x. (G) Alcian blue+ staining of acidic mucins and IHC staining of MUC5. 200x. Data are mean ± SD. *, p<0.05; **, p<0.01.

Figure 5. Pharmacological FGF21 inhibits HFD and KRAS^{G12D} induced pancreatic inflammation and ductal cell proliferation.

All the samples were described as in Figure 4A. (A) IHC staining of COX-2, F4/80, and CD3, as well as Sirius Red staining for collagen on pancreatic sections of *Kras*$^{G12D/+}$ mice. 200x. (B-C) qRT-PCR analysis of pancreatic *Cxcl5* and *Tgfb1* expression in *Kras*$^{G12D/+}$ mice with ND (n=4), HFD (n=4) or HFD+rhFGF21 (n=5). The age-matched ND-fed *fElas*^{CreERT} mice (n=5) served as a control. (D) Pancreatic RAS activity with the indicated treatments. (E) IHC staining of pancreatic cyclin D1 and Ki-67. 200x. Data are mean ± SD. *, p<0.05; **, p<0.01; ****, p<0.0001.

Figure 6. Pharmacological FGF21 inhibits HFD-promoted liver and adipose tissue inflammation

All mice were induced by TM at 70 days of age and then treated as indicated for 10 weeks prior to analyses. qRT-PCR analysis of *Ccl2, Ccl4, CD68, CD11b,* and *Tgfb1* in adipose tissues (A-E) and *Ccl2, Ccl4, CD68,* and *CD11b* in the liver (F-I) of *Kras*$^{G12D/+}$ mice with ND (n=5), HFD (n=6), or HFD+rhFGF21 (n=5). The ND-fed *fElas*^{CreERT} mice (n=5) were controls. Data are mean ± SD. *, p<0.05; **, p<0.01; ***, p<0.001.

Figure 7. Pharmacological FGF21 prevents liver metastasis and prolongs KRAS^{G12D} mice survival.

70-day-old mice were treated with TM to induce *fElas*^{CreERT} or *Kras*$^{G12D/+}$ expression, and then fed a ND or a HFD with or without rhFGF21 until they aged. The ND-fed *fElas*^{CreERT} mice (n=7) were controls. (A) Body weight of the *Kras*$^{G12D/+}$ mice with ND (n=7), HFD (n=7), or HFD+rhFGF21 treatment (n=7) until the HFD group aged. (B) Survival of the *Kras*$^{G12D/+}$ mice with ND (n=7), ND+rhFGF21 (n=10), HFD (n=7), or HFD+rhFGF21 treatment (n=7). The HFD-fed *Kras*$^{G12D/+}$ mice served as a control for statistical comparison. (C) Histological changes in pancreata of *Kras*$^{G12D/+}$ mice with the indicated treatments upon aging. 200x. (D) Liver metastasis. Upper panel, gross images of the livers. Middle panel, H&E stained sections. Lower panel, IHC analysis of CK19. (E) Schematic summary of the role of pancreatic FGF21 in the HFD and oncogenic KRAS mediated pancreatic tumorigenesis. 200x. Data are mean ± SD. *, p<0.05; ***, p<0.001; ****, p<0.0001.

ACCEPTED MANUSCRIPT

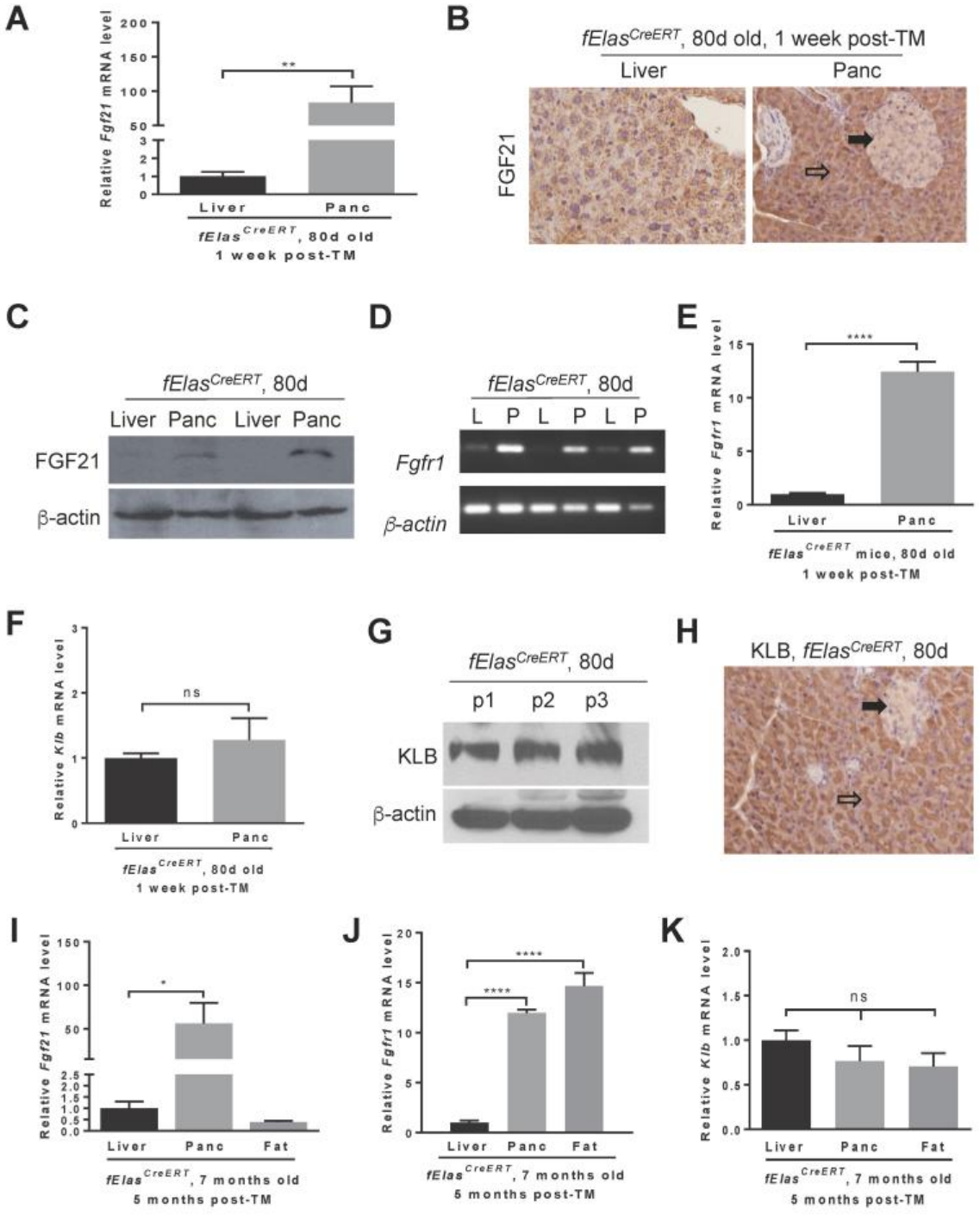
A
Relative Fgf21 mRNA level
200
150
100
50
3
2
1
0
**
Liver
Panc
fElasCreERT, 80d old
1 week post-TM
B
fElasCreERT, 80d old, 1 week post-TM
Liver
Panc
FGF21
C
fElasCreERT, 80d
Liver Panc Liver Panc
FGF21
β-actin
D
fElasCreERT, 80d
L P L P L P
Fgfr1
β-actin
E
Relative Fgfr1 mRNA level
15
10
5
0
****
Liver
Panc
fElasCreERT mice, 80d old
1 week post-TM
F
Relative Klb mRNA level
3
2
1
0
ns
Liver
Panc
fElasCreERT, 80d old
1 week post-TM
G
fElasCreERT, 80d
p1 p2 p3
KLB
β-actin
H
KLB, fElasCreERT, 80d
I
Relative Fgf21 mRNA level
150
100
50
2.5
2.0
1.5
1.0
0.5
0.0
*
Liver
Panc
Fat
fElasCreERT, 7 months old
5 months post-TM
J
Relative Fgfr1 mRNA level
20
15
10
5
0
****
****
Liver
Panc
Fat
fElasCreERT, 7 months old
5 months post-TM
K
Relative Klb mRNA level
2.0
1.5
1.0
0.5
0.0
ns
Liver
Panc
Fat
fElasCreERT, 7 months old
5 months post-TM

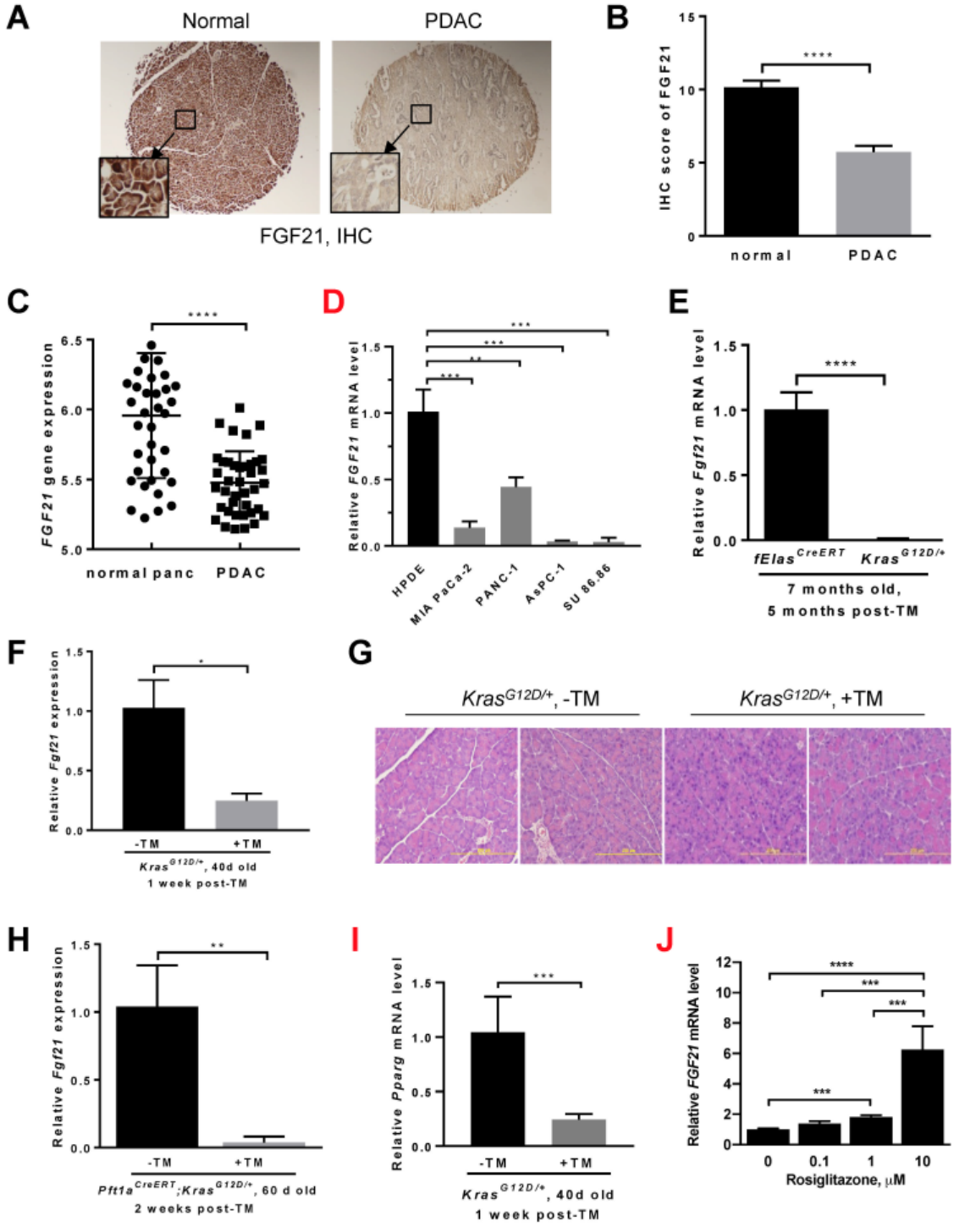
A
Normal
PDAC
FGF21, IHC
B
IHC score of FGF21
normal
PDAC
C
FGF21 gene expression
normal panc
PDAC
D
Relative FGF21 mRNA level
HPDE
MIA PaCa-2
PANC-1
AsPC-1
SU 86.86
E
Relative Fgf21 mRNA level
fElas CreERT
Kras G12D/+
7 months old,
5 months post-TM
F
Relative Fgf21 expression
-TM
+TM
Kras G12D/+, 40d old
1 week post-TM
G
Kras G12D/+, -TM
Kras G12D/+, +TM
H
Relative Fgf21 expression
-TM
+TM
Pft1a CreERT;Kras G12D/+, 60 d old
2 weeks post-TM
I
Relative Pparg mRNA level
-TM
+TM
Kras G12D/+, 40d old
1 week post-TM
J
Relative FGF21 mRNA level
Rosiglitazone, μM

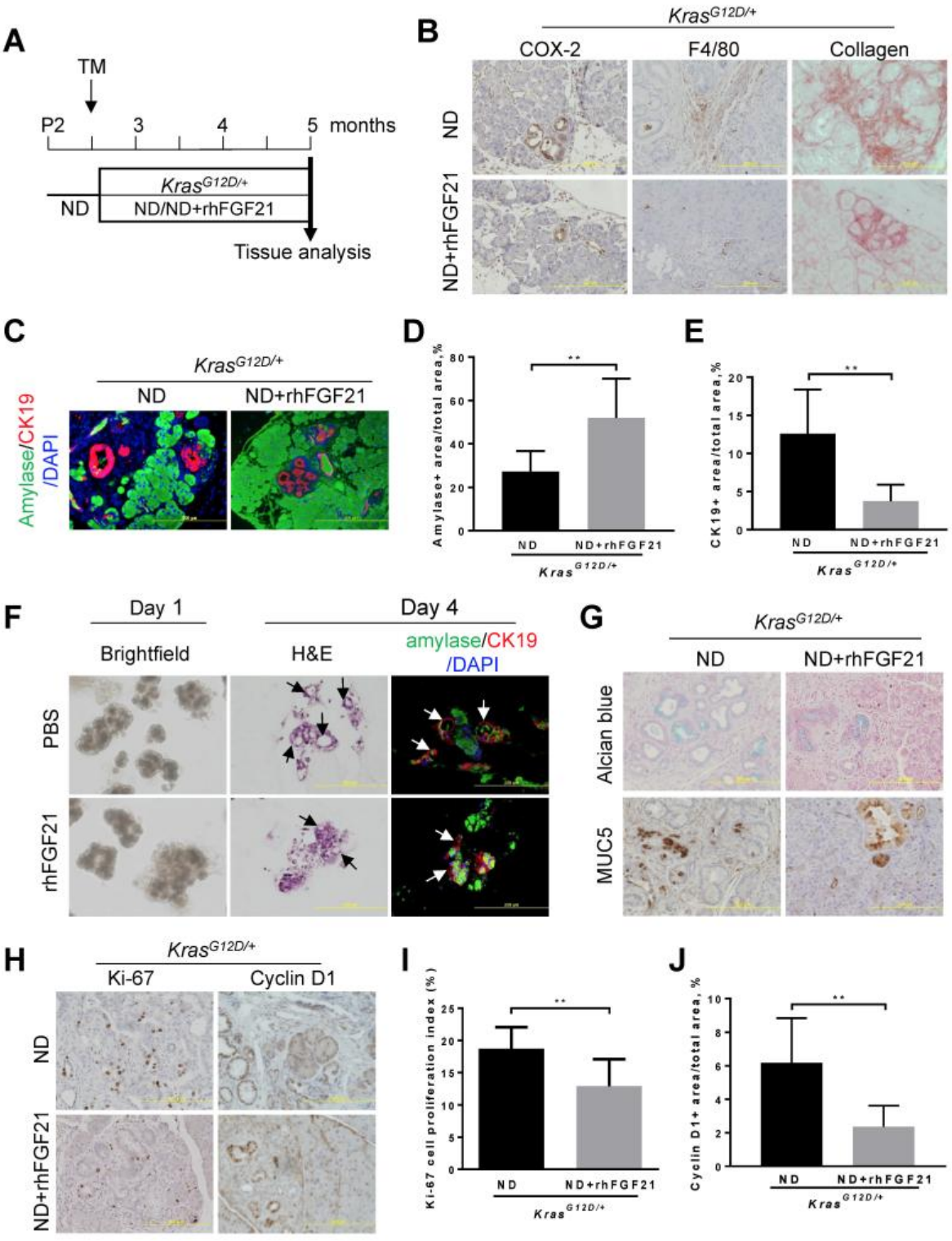
A
TM
P2
3
4
5 months
ND
KrasG12D/+
ND/ND+rhFGF21
Tissue analysis
B
KrasG12D/+
COX-2
F4/80
Collagen
ND
ND+rhFGF21
C
KrasG12D/+
ND
ND+rhFGF21
Amylase/CK19
/DAPI
D
Amylase+ area/total area,%
ND
ND+rhFGF21
KrasG12D/+
E
CK19+ area/total area,%
ND
ND+rhFGF21
KrasG12D/+
F
Day 1
Day 4
Brightfield
H&E
amylase/CK19
/DAPI
PBS
rhFGF21
G
KrasG12D/+
ND
ND+rhFGF21
Alcian blue
MUC5
H
KrasG12D/+
Ki-67
Cyclin D1
ND
ND+rhFGF21
I
Ki-67 cell proliferation index (%)
ND
ND+rhFGF21
KrasG12D/+
J
Cyclin D1+ area/total area, %
ND
ND+rhFGF21
KrasG12D/+

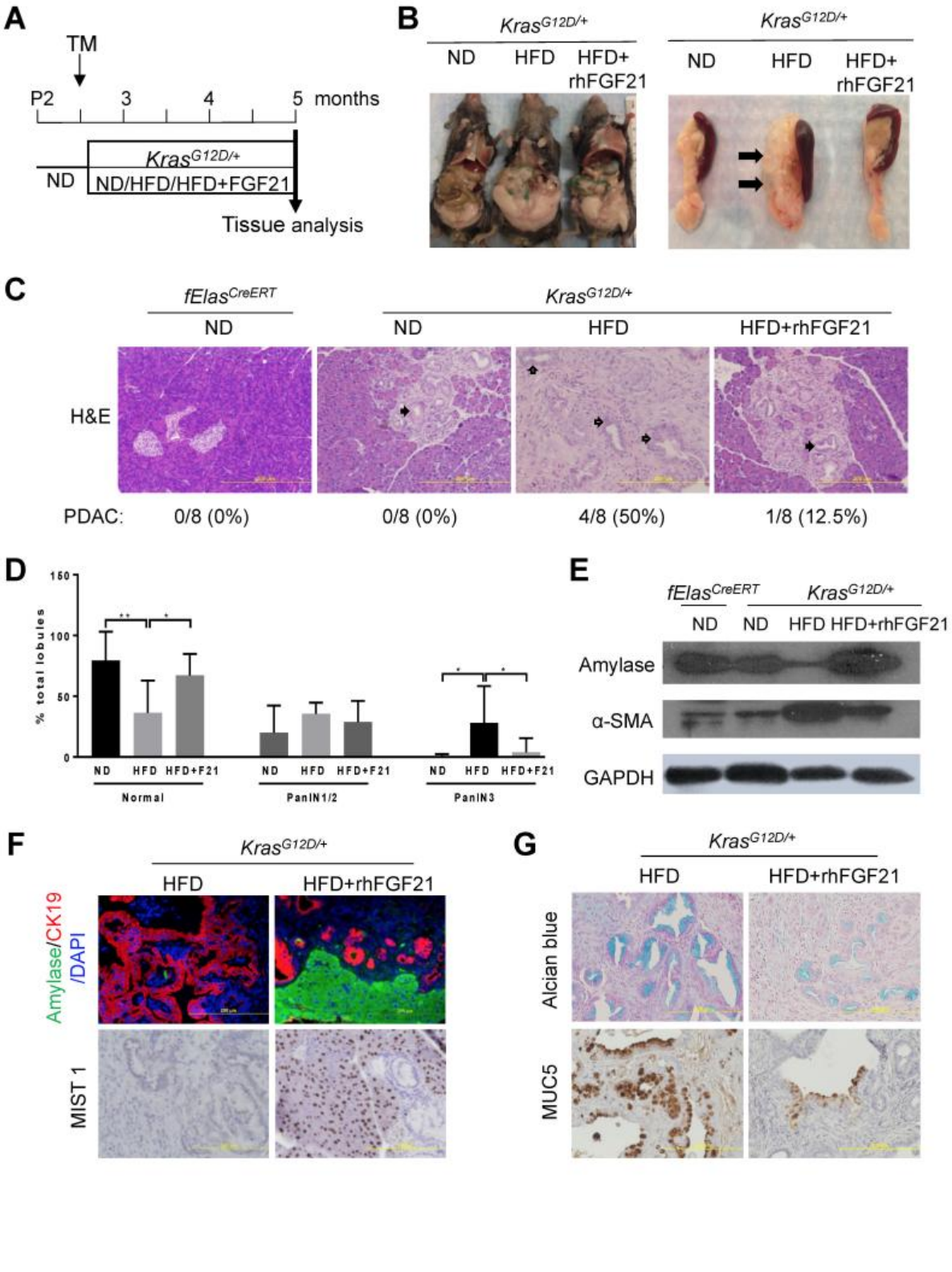
A
TM
P2
3
4
5 months
Kras^G12D/+
ND
ND/HFD/HFD+FGF21
Tissue analysis
B
Kras^G12D/+
ND
HFD
HFD+ rhFGF21
Kras^G12D/+
ND
HFD
HFD+ rhFGF21
C
fElas^CreERT
Kras^G12D/+
ND
ND
HFD
HFD+rhFGF21
H&E
PDAC:
0/8 (0%)
0/8 (0%)
4/8 (50%)
1/8 (12.5%)
D
% total lobules
ND
HFD
HFD+F21
Normal
PanIN1/2
PanIN3
E
fElas^CreERT
Kras^G12D/+
ND
ND
HFD
HFD+rhFGF21
Amylase
α-SMA
GAPDH
F
Kras^G12D/+
HFD
HFD+rhFGF21
Amylase/CK19 /DAPI
MIST 1
G
Kras^G12D/+
HFD
HFD+rhFGF21
Alcian blue
MUC5

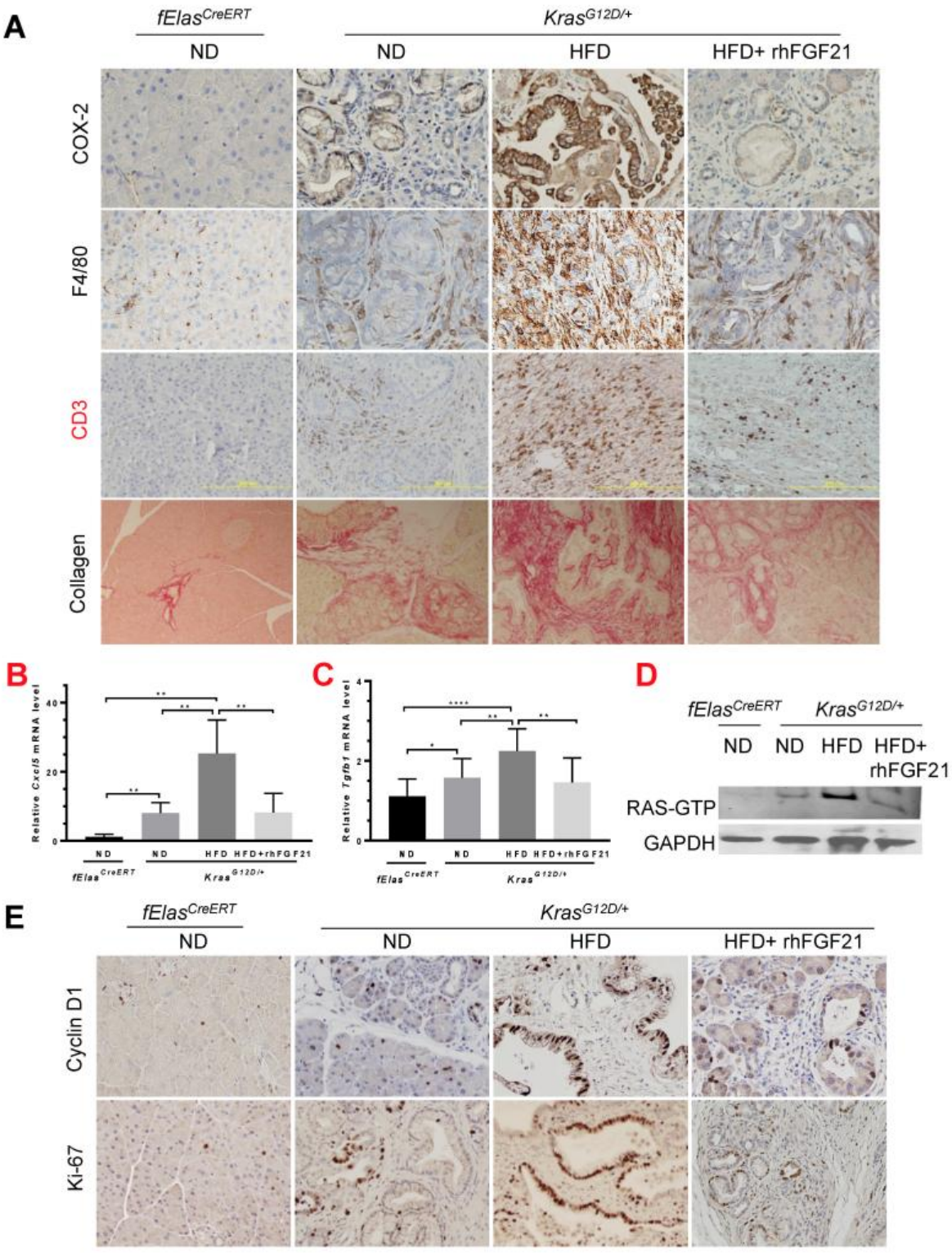
A
fElasCreERT
KrasG12D/+
ND
ND
HFD
HFD+ rhFGF21
COX-2
F4/80
CD3
Collagen
B
Relative Cxcl5 mRNA level
C
Relative Tgfb1 mRNA level
D
fElasCreERT
KrasG12D/+
ND
ND
HFD
HFD+ rhFGF21
RAS-GTP
GAPDH
E
fElasCreERT
KrasG12D/+
ND
ND
HFD
HFD+ rhFGF21
Cyclin D1
Ki-67

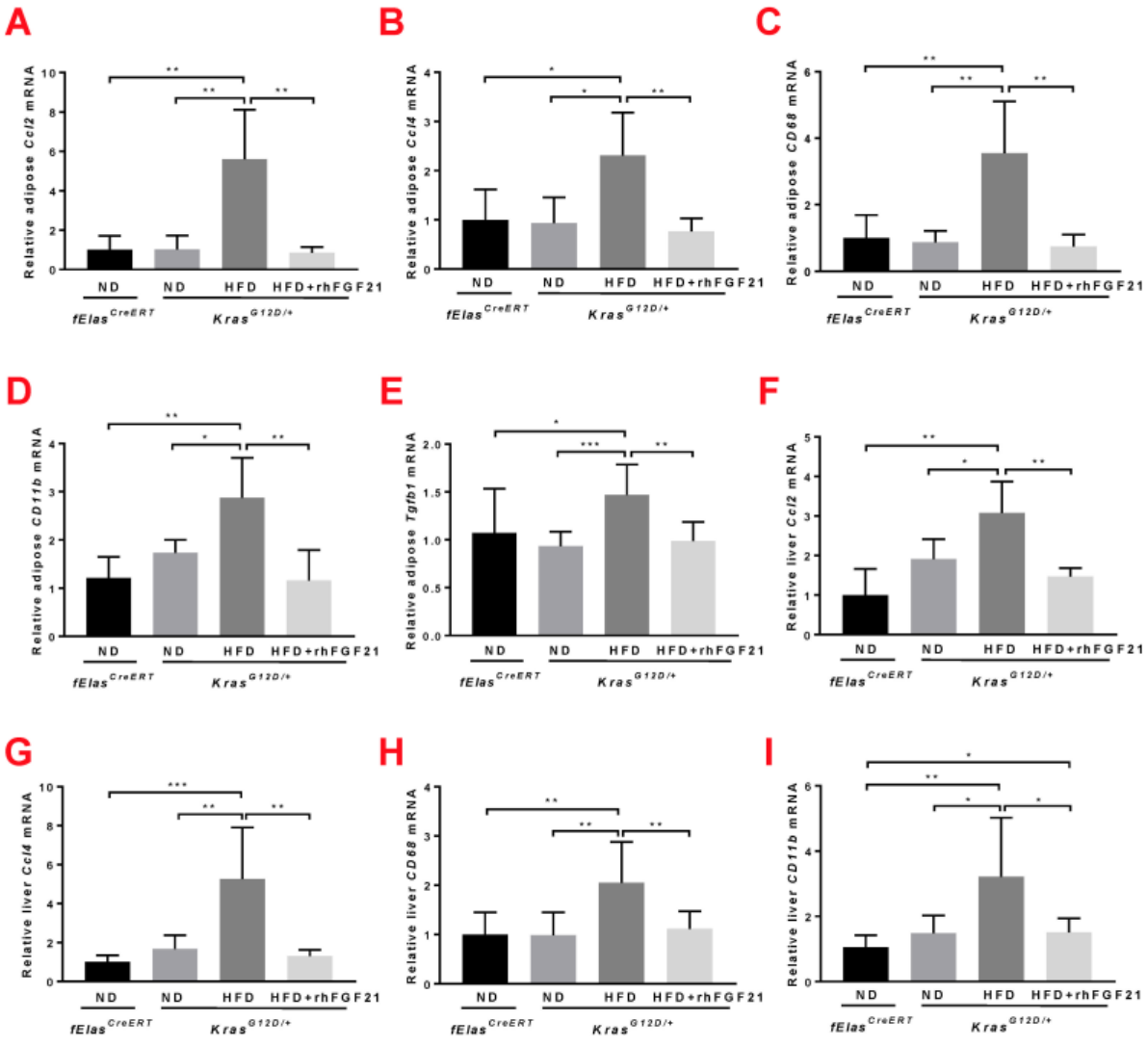
A
Relative adipose Ccl2 mRNA
B
Relative adipose Ccl4 mRNA
C
Relative adipose CD68 mRNA
D
Relative adipose CD11b mRNA
E
Relative adipose Tgfb1 mRNA
F
Relative liver Ccl2 mRNA
G
Relative liver Ccl4 mRNA
H
Relative liver CD68 mRNA
I
Relative liver CD11b mRNA
ND
ND
HFD
HFD+rhFGF21
fElas CreERT
Kras G12D/+

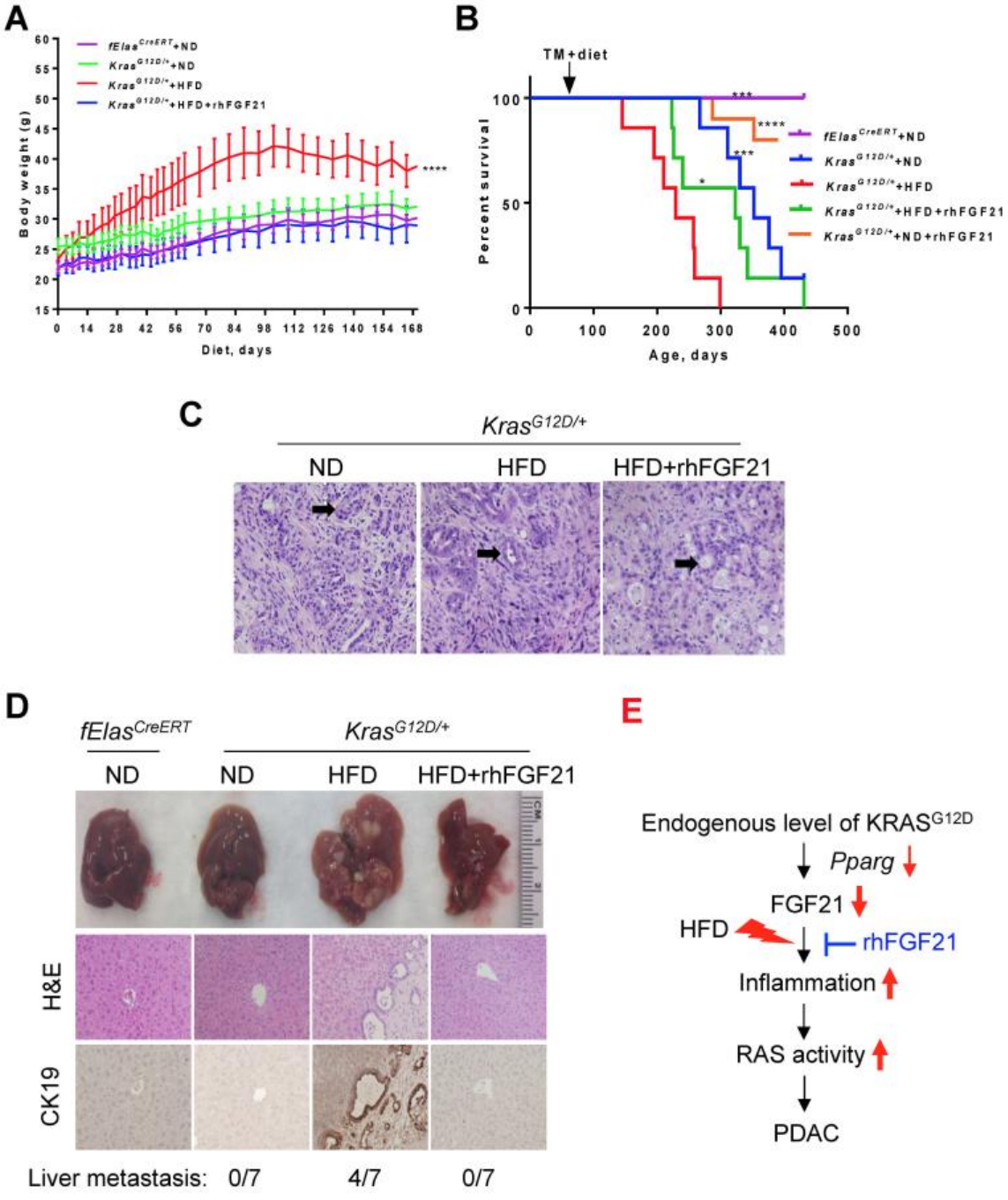
A
Body weight (g)
Diet, days
fElas^CreERT+ND
Kras^G12D/+ND
Kras^G12D/+HFD
Kras^G12D/+HFD+rhFGF21
****
B
TM+diet
Percent survival
Age, days
fElas^CreERT+ND
Kras^G12D/+ND
Kras^G12D/+HFD
Kras^G12D/+HFD+rhFGF21
Kras^G12D/+ND+rhFGF21
C
Kras^G12D/+
ND
HFD
HFD+rhFGF21
D
fElas^CreERT
Kras^G12D/+
ND
ND
HFD
HFD+rhFGF21
H&E
CK19
Liver metastasis: 0/7 4/7 0/7
E
Endogenous level of KRAS^G12D
Pparg
FGF21
HFD
rhFGF21
Inflammation
RAS activity
PDAC

ACCEPTED MANUSCRIPT

WHAT YOU NEED TO KNOW

BACKGROUND AND CONTEXT: A high-fat diet (HFD) promotes obesity, which increases the risk of pancreatic cancer. In mice, a HFD and expression of oncogenic KRAS lead to the development of pancreatic cancer. We investigated how the expression of oncogenic KRAS regulates fibroblast growth factor 21 (FGF21), which prevents obesity, and the effects of FGF21 administration on pancreatic tumorigenesis.

NEW FINDINGS: Normal acinar cells from mice and humans express high levels of FGF21. In mice, acinar expression of oncogenic KRAS significantly reduces FGF21 expression. When these mice are placed on a HFD, they develop extensive inflammation, pancreatic cysts, pancreatic intraepithelial neoplasias, and pancreatic adenocarcinomas—all were reduced by injection of FGF21. FGF21 reduces HFD-promoted RAS activity.

LIMITATIONS: These studies were performed in mice—more studies of humans are needed.

IMPACT: FGF21 is downregulated by oncogenic KRAS. FGF21 might be given to patients for the prevention or treatment of pancreatic cancer.

ACCEPTED MANUSCRIPT

ACCEPTED MANUSCRIPT

Lay Summary

A high-fat diet promotes development of pancreatic cancer. We found that acinar cells that express oncogenic KRAS reduce expression of fibroblast growth factor 21. In mice on a high-fat diet, injection of fibroblast growth factor 21 reduces pancreatic inflammation and tumor development.

ACCEPTED MANUSCRIPT

ACCEPTED MANUSCRIPT

SUPPLEMENTAL INFORMATION FOR:

Oncogenic KRAS Reduces Expression of FGF21 in Acinar Cells to Promote Pancreatic Tumor Development in Mice on a High-Fat Diet

Yongde Luo[1,2,*], Yaying Yang[3, *], Muyun Liu[3,*], Dan Wang[2], Feng Wang[4], Yawei Bi[2], Juntao Ji[2], Suyun Li[2], Yan Liu[5], Rong Chen[6], Haojie Huang[5], Xiaojie Wang[1], Agnieszka K. Swidnicka-Siergiejko[5], Tobias Janowitz[7], Semir Beyaz[7], Guoqiang Wang[2], Sulan Xu[2], Agnieszka B. Bialkowska[2], Catherine K. Luo[2], Christoph L. Pin[8], Guang Liang[1], Xiongbin Lu[9], Maoxin Wu[10], Kenneth R. Shroyer[10], Robert A. Wolff[3], William Plunkett[6], Baoan Ji[11], Zhaoshen Li[12], Ellen Li[2], Xiaokun Li[1], Vincent W. Yang[2], Craig D. Logsdon[3,5,§], James L. Abbruzzese[3,13,§] & Weiqin Lu[2,3,§]

[1]School of Pharmaceutical Science, Wenzhou Medical University, Wenzhou, Zhejiang, China.

[2]Department of Medicine, [10]Department of Pathology, Stony Brook University, Stony Brook, NY, 11794, USA

[3]Department of Gastrointestinal Medical Oncology, [5]Department of Cancer Biology, [6]Department of Experimental Therapeutics, University of Texas, MD Anderson Cancer Center, Houston, TX, 77030, USA

[4]Sun Yat-Sen University Cancer Center, State Key Laboratory of Oncology in South China, Collaborative Innovation Center for Cancer Medicine, Guangzhou, 510060, China.

[7]Cold Spring Harbor Laboratory, Cold Spring Harbor, NY, 11724, USA

[8]Departments of Pediatrics, Oncology, and Physiology and Pharmacology, Schulich School of Medicine, University of Western Ontario Children's Health Research Institute, London, ON, Canada N5C 2V5

ACCEPTED MANUSCRIPT

[9]Department of Medical and Molecular Genetics, Indiana University School of Medicine. Indianapolis, IN, USA

[11]Department of Biochemistry and Molecular Biology, Mayo Clinic, Jacksonville, FL, USA

[12]Department of Gastroenterology, Changhai Hospital, Shanghai, China

[13]Division of Medical Oncology, Department of Medicine, Duke Cancer Institute, Duke University, Durham, NC, 27710, USA

[*] Authors share co-first authorship.

[§]Authors share co-senior authorship

ACCEPTED MANUSCRIPT

CONTENTS

1. Supplementary Figures

Supplementary Figure 1

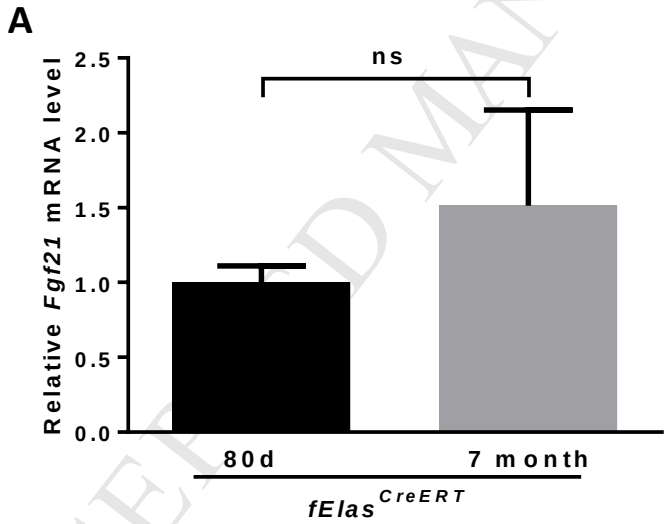

Supplementary Figure 1, relating to Figure 1. (A) qRT-PCR analysis of the expression levels of *Fgf21* in pancreatic tissues from 80-day-old *fElas*^{CreERT} mice (n=4) one week post-TM induction, and from 7-month-old *fElas*^{CreERT} mice (n=6) five months post-TM induction. All the mice were fed a normal diet for the duration of the experiments. Results indicate that pancreatic *Fgf21* gene expression remains

unchanged with age in the *fElas*^{CreERT} mice. Results are expressed as mean ± SD. *p* values are determined by the Student's *t*-test. ns, not significant.

ACCEPTED MANUSCRIPT

Supplementary Figure 2

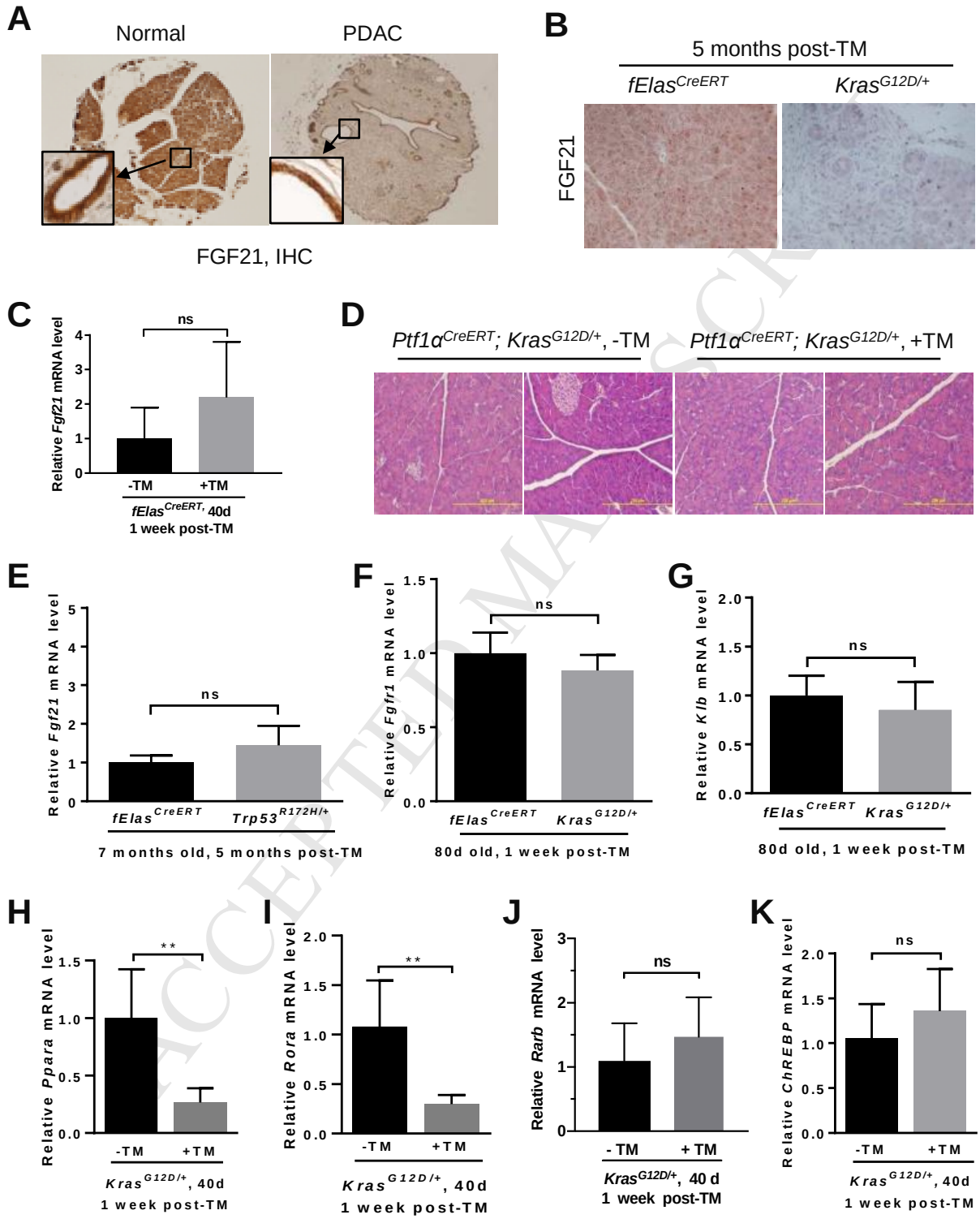

Supplementary Figure 2, relating to Figure 2. (A) Representative IHC staining of FGF21 in tissue arrays of normal human pancreata (left) and PDAC specimens (right) (40x). *Inset*: normal ducts, 200x. (B) Representative IHC analysis of FGF21 levels in 7-month-old $Kras^{G12D/+}$ mice 5 months post-TM induction. 200x. (C) qRT-PCR analysis for *Fgf21* expression in 40-day-old $fElas^{CreERT}$ mice one week after TM induction (n=11) or without TM induction (n=6). (D) Representative H&E staining of the pancreatic tissue sections in the $Ptf1\alpha^{CreERT};Kras^{G12D/+}$ mice with or without TM induction as in Figure 2H. (E) qRT-PCR analysis of *Fgf21* expression in pancreatic tissues obtained from 7-month-old $fElas^{CreERT}$ (n=3) and $Trp53^{R172H/+}$ (n=4) mice five months post-TM induction. (F) qRT-PCR analysis of pancreatic *Fgfr1* expression in 80-day-old $Kras^{G12D/+}$ mice (n=5) or $fElas^{CreERT}$ mice (n=4), one week post-TM treatment. (G) qRT-PCR analysis for pancreatic *Klb* expression in 80-day-old adult $Kras^{G12D/+}$ mice (n=9) or $fElas^{CreERT}$ mice (n=6), one week after TM treatment. (H-K) qRT-PCR analysis for pancreatic *Ppara, Rora, Rarb, and ChREBP* expression in 40-day-old $Kras^{G12D/+}$ mice (n=6) or $fElas^{CreERT}$ mice (n=6) one week post-TM induction. All the mice were fed a ND. Results are expressed as mean ± SD. *p* values are determined by the Student's *t*-test. ns: no significance. **, $p<0.01$.

Supplementary Figure 3

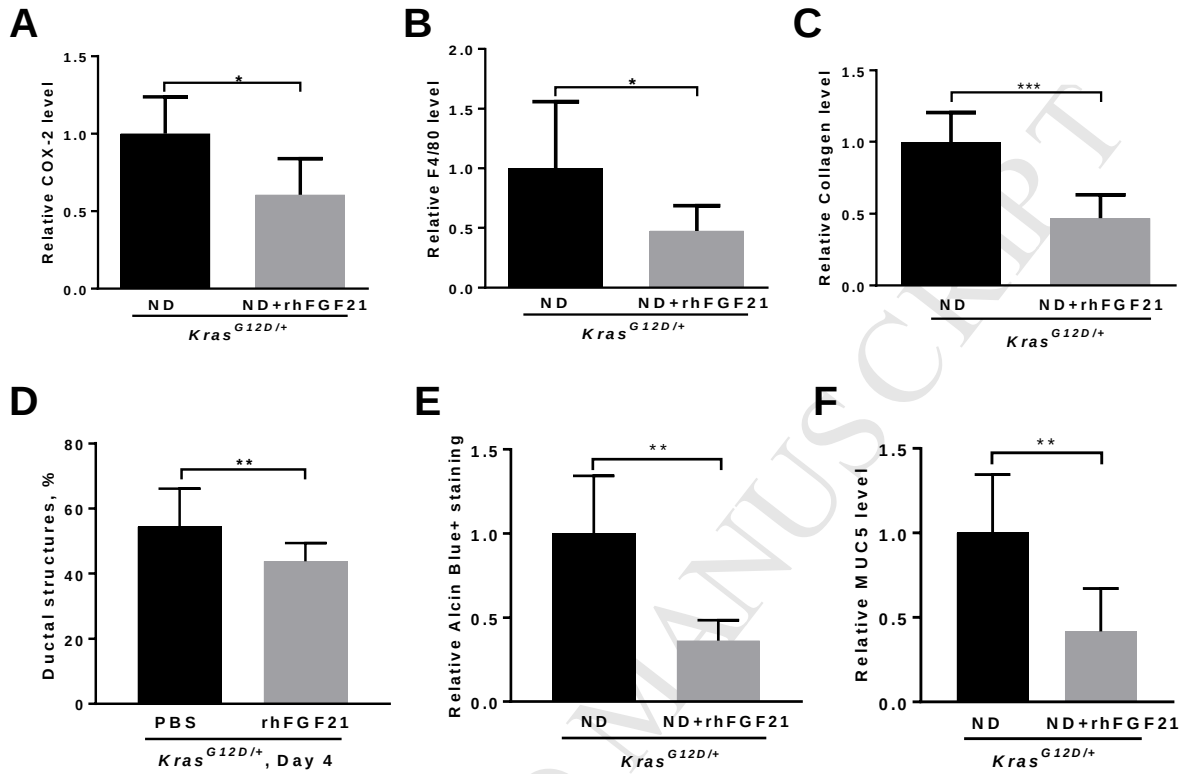

Supplementary Figure 3, relating to Figure 3. (A-B) Quantitative analysis of COX-2+ or F4/80+ areas in the *Kras*$^{G12D/+}$ mice with ND (n=4) or ND+rhFGF21 (n=4) treatment using images as represented in Figure 3B. (C) Quantitative analysis of Collagen+ areas in the *Kras*$^{G12D/+}$ mice with ND (n=6) or ND+rhFGF21 (n=5) treatment using images as represented in Figure 3B. (D) Quantification of the percentage of tubular ductal structures in the entire acinar clusters on day 4 after the indicated treatments with three independent experiments as shown in Figure 3F. (E) Quantitative analysis of Alcian blue+ areas over total areas in the *Kras*$^{G12D/+}$ mice with ND (n=6) or ND+rhFGF21 (n=6) treatment using images as represented in Figure 3G. (F) Quantitative analysis of MUC5+ areas in the *Kras*$^{G12D/+}$ mice with ND (n=5) or ND+rhFGF21 (n=5) treatment

using images as represented in Figure 3G. Fiji ImageJ software was used to obtain image data for statistical analyses. Results are expressed as mean ± SD. *p* values are determined by the Student's *t*-test. *, $p<0.05$; **, $p<0.01$; ***, $p<0.001$.

ACCEPTED MANUSCRIPT

Supplementary Figure 4

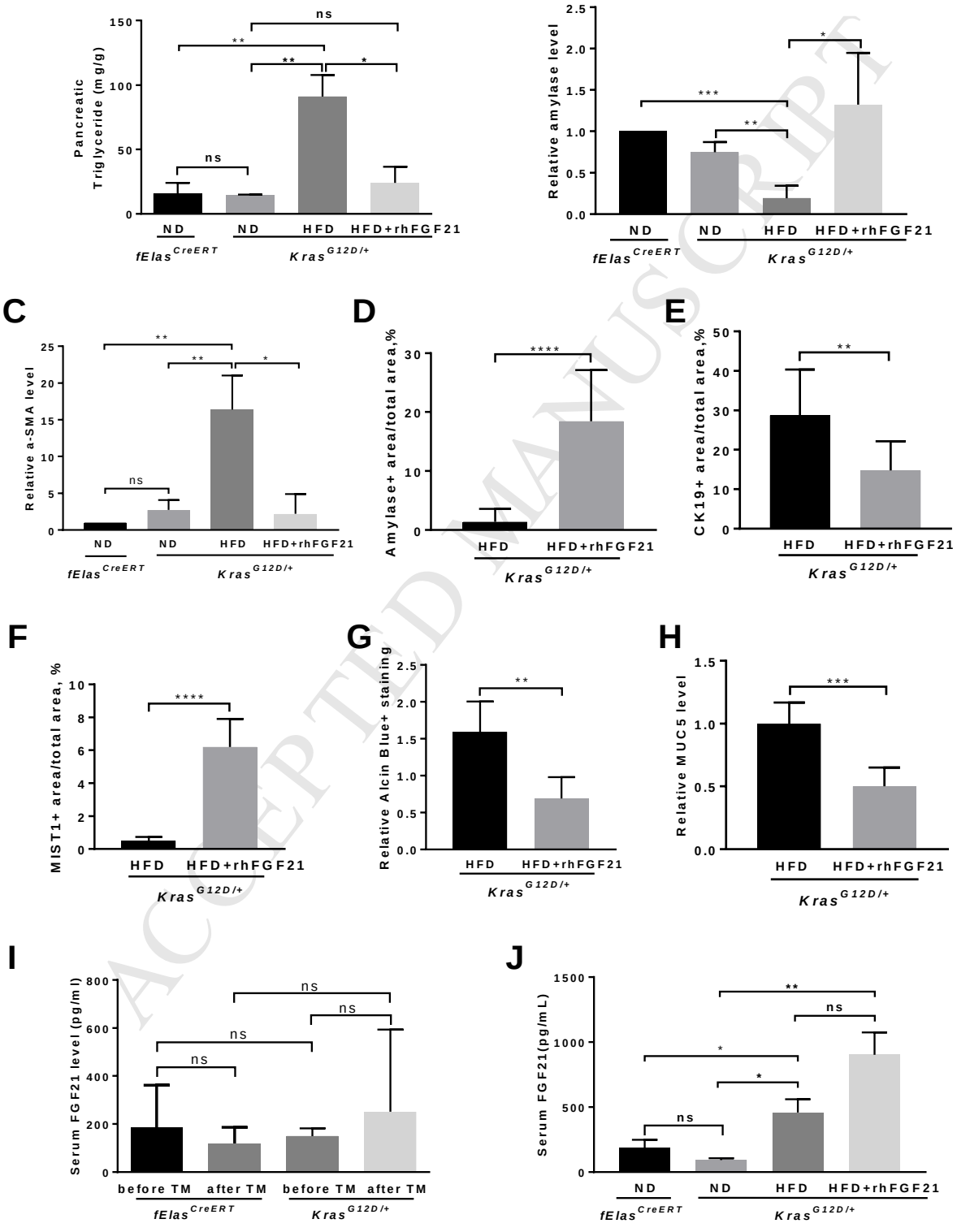

ACCEPTED MANUSCRIPT

Supplementary Figure 4, relating to Figure 4. (A) Triglyceride levels in the pancreata were quantitatively analyzed in *Kras*$^{G12D/+}$ mice with the indicated treatments for 10 weeks. (B-C) Quantitative analysis of amylase or α-SMA protein levels from three independent Western blot data as represented in Figure 4E. (D-E) Quantitative analyses of amylase+ or CK19+ areas from the Co-IF imaging data from four different mice in each group as represented in Figure 4F. (F) Quantitative analysis of MIST1+ areas from IHC data of five different mice in each group as represented in Figure 4F. (G-H) Quantitative analysis of Alcian blue+ or MUC5+ areas over total areas using images after HFD (n=3) or HFD+rhFGF21 (n=3) treatment as represented in Figure 4G. (I) Serum FGF21 levels from the *fElas*^{CreERT} mice before (n=11) and one week post-TM treatment (n=11) and from the *Kras*$^{G12D/+}$ mice before (n=29) and one week post-TM treatment (n=31). Mice at 70 days of age were treated with TM and serum FGF21 levels were measured using Quantikine FGF21 ELISA kits. (J) 70-day-old *Kras*$^{G12D/+}$ and *fElas*^{CreERT} mice were treated with TM for 5 consecutive days followed by 10 weeks of the indicated treatments. Serum FGF21 levels were then compared using Quantikine FGF21 ELISA kits in the *Kras*$^{G12D/+}$ mice and the *fElas*^{CreERT} mice. Data from 4I and 4J suggest that pancreatic *Fgf21* gene silencing by Kras^{G12D} did not impact systemic FGF21 levels. No significant differences in serum FGF21 levels were observed in the HFD-fed *Kras*$^{G12D/+}$ mice regardless of rhFGF21 treatment, even though an increased tendency of serum FGF21 levels were observed in the group with concurrent HFD and rhFGF21 treatment, suggesting that rhFGF21 treatment did not significantly alter serum FGF21 levels. However, *Kras*$^{G12D/+}$ mice treated with either a HFD or HFD+rhFGF21 had significantly higher levels of serum FGF21 compared to that of the ND-fed

Kras$^{G12D/+}$ mice, suggesting that the increased serum FGF21 was induced mainly by HFD. Fiji ImageJ software was used to obtain data from IHC images for statistical analysis. Results are expressed as mean ± SD. *p* values are determined by the Student's *t*-test. ns, not significant, *, p<0.05; **, p<0.01; ***, p<0.001; ****, p<0.0001.

ACCEPTED MANUSCRIPT

Supplementary Figure 5

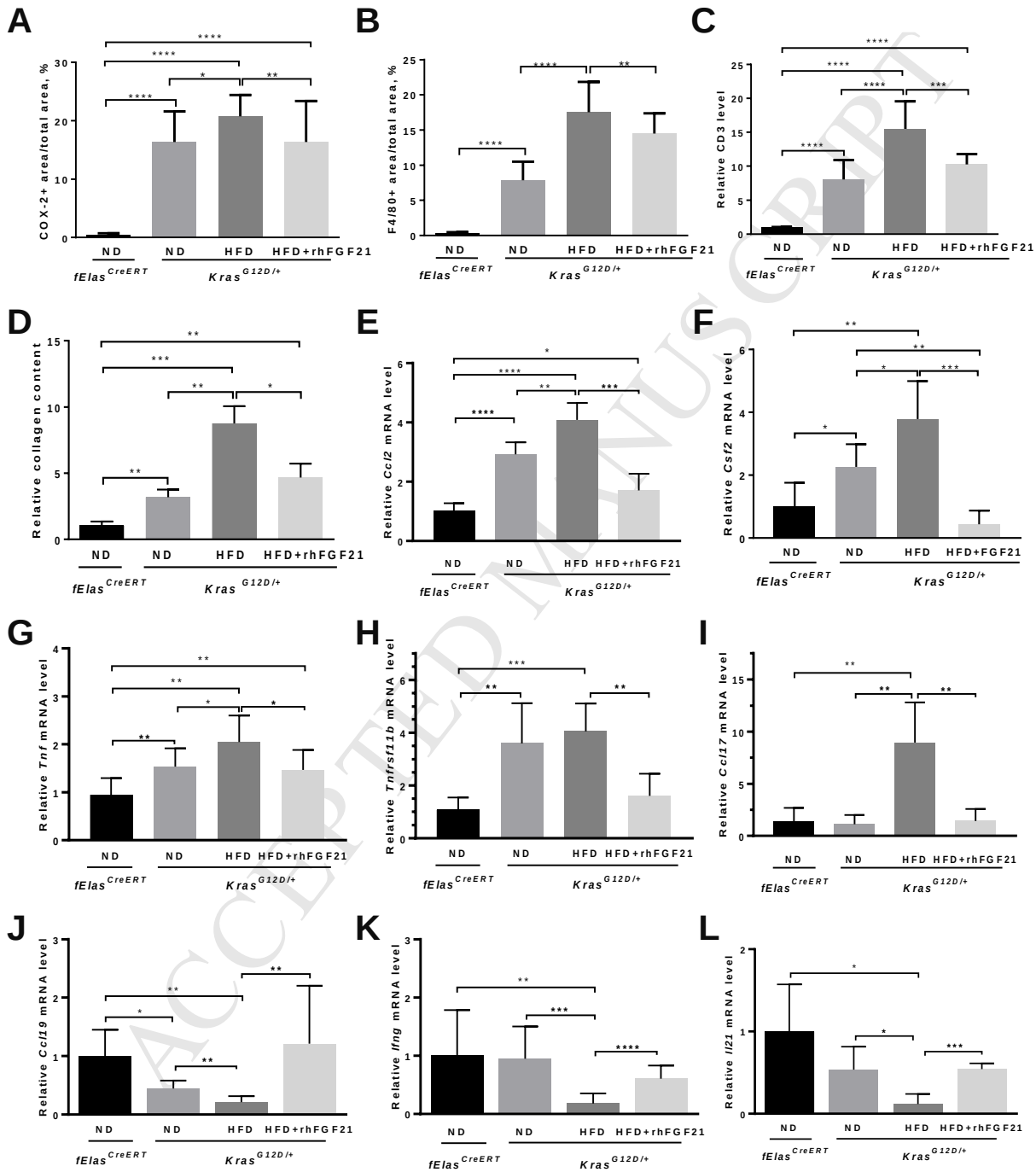

ACCEPTED MANUSCRIPT

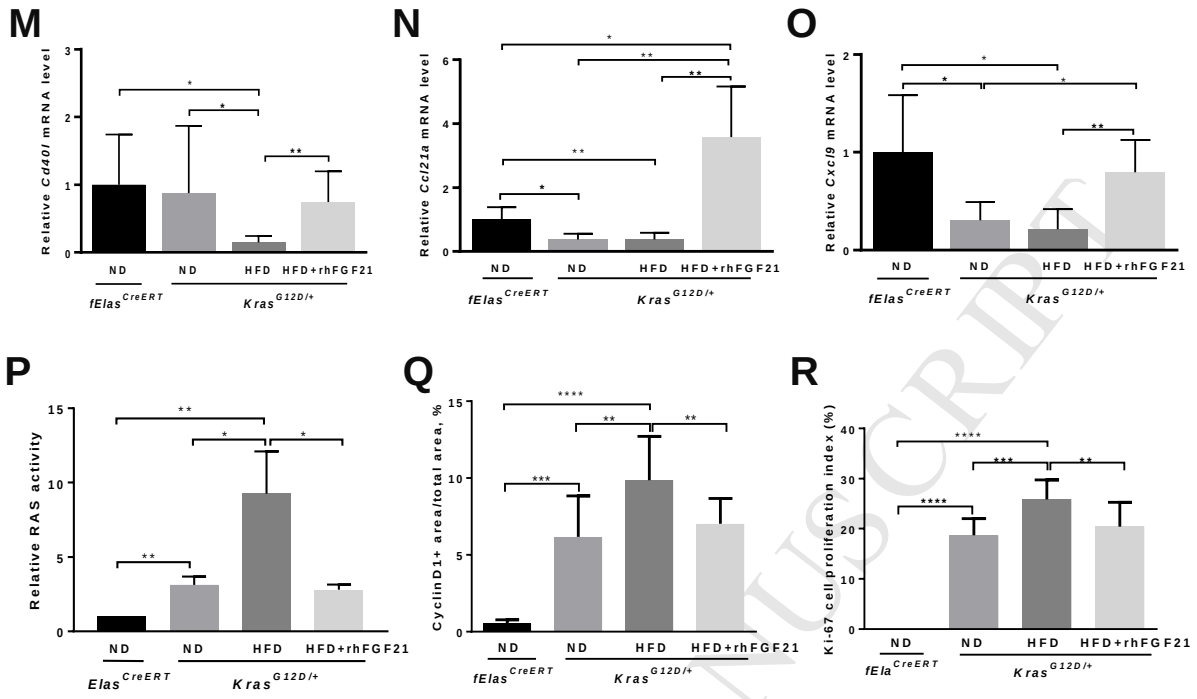

Supplementary Figure 5, relating to Figure 5. All tissue samples in the following analyses were described as in Figure 4A. The ND-fed *fElas*^{CreERT} mice (n=4) served as normal control. (A-D) Quantitative analysis of COX-2+, F4/80+, CD3+, and collagen-positive areas in *Kras*$^{G12D/+}$ mice with ND (n=4), HFD (n=4) or HFD+rhFGF21 (n=5) treatment as represented in Figure 5A. (E-O) qRT-PCR analysis of pancreatic *Ccl2, Csf2, Tnf, Tnfrsf11b, Ccl17*, *Ccl19*, *Ifng*, *Il21, Cd40l, Ccl21a, and Cxcl9* in the *Kras*$^{G12D/+}$ mice with ND (n=4), HFD (n=4) or HFD+rhFGF21 (n=5) treatment. (P) Quantitative analysis of pancreatic RAS activity from three independent RAS activity experiments as represented in Figure 5D. (Q) Quantitative analysis of Cyclin D1+ areas in the pancreata of *Kras*$^{G12D/+}$ mice with ND (n=4), HFD (n=4) or HFD+rhFGF21 (n=4) treatment as represented in the upper panel of Figure 5E. (R) Quantitative analysis of Ki-67+ areas in the pancreata of *Kras*$^{G12D/+}$ mice with ND (n=4), HFD (n=6) or

HFD+rhFGF21 (n=6) treatment as represented in the lower panel of Figure 5E. Fiji ImageJ software was used to obtain data from IHC images for statistical analysis. Results are expressed as mean ± SD. *p* values are determined by the Student's *t*-test. *, p<0.05; **, p<0.01; ***, p<0.001; ****, p<0.0001.

ACCEPTED MANUSCRIPT

Supplementary Figure 6

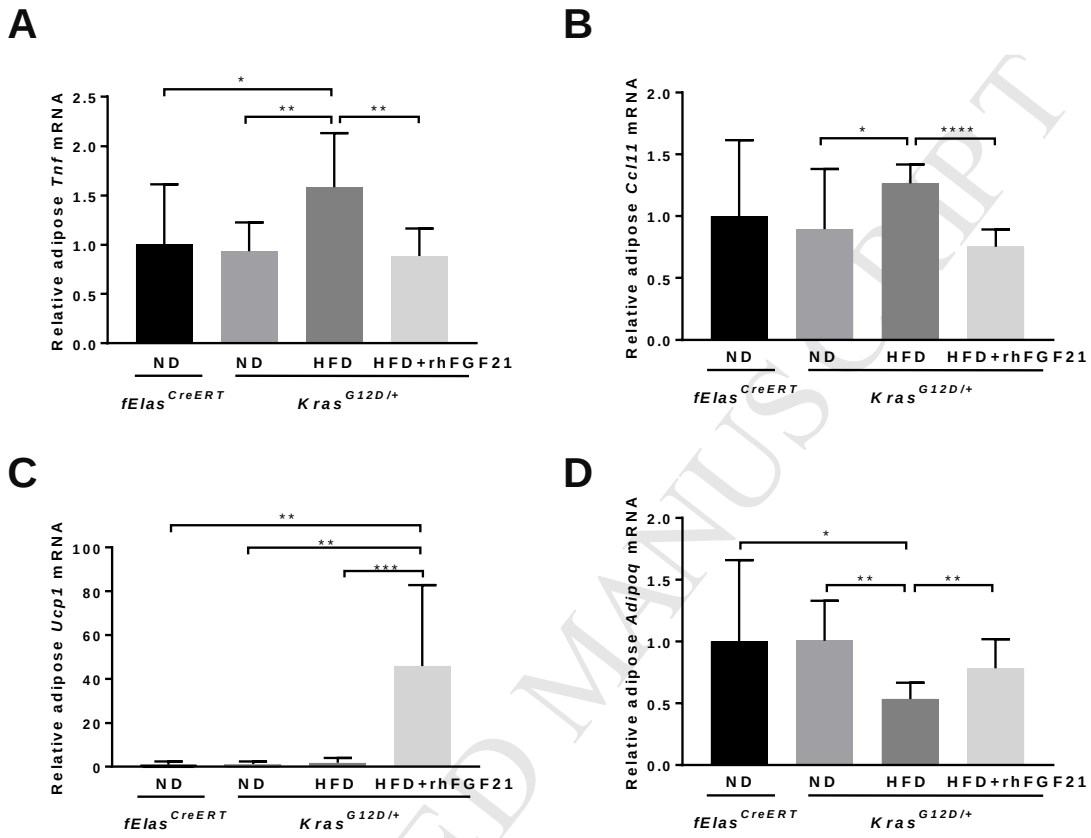

Supplementary Figure 6, relating to Figure 6. All mice were induced by TM at 70 days of age and then received the indicated treatments for 10 weeks prior to qRT-PCR analysis. (A-D) qRT-PCR analyses of adipose *Tnf, Ccl11, Ucp1,* and *Adipoq gene expression* in *Kras$^{G12D/+}$ mice* with ND (n=5), HFD (n=6) or HFD+rhFGF21 (n=5). The ND-fed *fElas^{CreERT}* mice (n=5) served as a control. Results are expressed as mean ± SD. *p* values are determined by the Student's *t*-test. *, p<0.05; **, p<0.01; ***, p<0.001; ****, p<0.0001.

Supplementary Figure 7

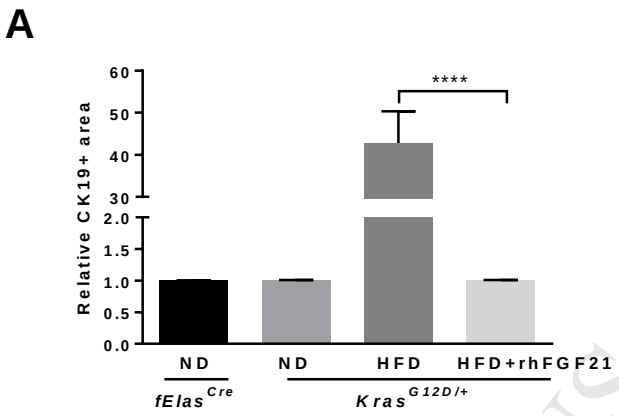

Supplementary Figure 7, relating to Figure 7. (A) Quantitative analysis of CK19+ areas in the representative liver images of *Kras*$^{G12D/+}$ mice with ND (n=4), HFD (n=6) or HFD+rhFGF21 (n=6) treatment as represented in Figure 7D (lower panel). Results are expressed as mean ± SD. *p* values are determined by the Student's *t*-test. ****, $p<0.0001$.

ACCEPTED MANUSCRIPT

2. Supplementary Table 1

Supplementary Table 1. List of primer sets for qRT-PCR assessment of expression of different genes.

Gene symbol	Forward primer	Reverse primer
Fgf21	5'-TTCAAATCCTGGGTGTCAAA-3'	5'-CAGCAGCAGTTCTCTGAAGC-3'
h*FGF21*	5'-CGGGAGCTGCTTCTTGAGGA-3'	5'-CTGGTAGTGGCAGGAAGCGA-3'
Fgfr1	5'-CTGAAGGAGGGTCATCGAAT-3'	5'-GTCCAGGTCTTCCACCAACT-3'
Klb	5'-CAGAGAAGGAGGAGGTGAGG-3'	5'-CAGCACCTGCCTTAAGTTGA-3'
β-actin	5'-CGGTTCCGATGCCCTGAGGCTCTT-3'	5'-CGTCACACTTCATGATGGAATTGA-3'
18S rRNA	5'-GCAATTATTCCCCATGAACG-3'	5'-GGCCTCACTAAACCATCCAA-3'
Cxcl5	5'-GGAGCTGCGTTGTGTTTGCT-3'	5'-ACTTCCACCGTAGGGCACTG-3'
Tgfβ1	5'-CCCGTGGCTTCTAGTGCTGA-3'	5'-ACAGGATCTGGCCACGGATG-3'
Ccl2	5'-GCATCTGCCCTAAGGTCTTC-3'	5'-AAGTGCTTGAGGTGGTTGTG-3'
Csf2	5'-TTTACTTTTCCTGGGCATTG-3'	5'-TAGCTGGCTGTCATGTTCAA-3'
Tnf	5'-ATGAGAAGTTCCCAAATGGC-3'	5'-CTCCACTTGGTGGTTTGCTA-3'
Ccl17	5'-CCGAGAGTGCTGCCTGGATT-3'	5'-GAGCTTGCCCTGGACAGTCA-3'
Ccl19	5'-TCAGCTCTGTGCACCTCCAG-3'	5'-GCTCCTTCTGGTGCTGTTGC-3'
Tnfrsf11b	5'-CATCTCGGCCACTCGAACCT-3'	5'-AGGAGCTGCTCGCTCGATTT-3'
Ccl4	5'-AGCAACACCATGAAGCTCTG-3'	5'-CCGGGAGGTGTAAGAGAAAC-3'
CD68	5'-CCGGACCCACAACTGTCACT-3'	5'-GAGGGCCAACAGTGGAGGAT-3'
CD11b	5'-GCCTCCCTTTGCTCTGTGGA-3'	5'-CTCGAGGCAAGGGACACACT-3'
Ucp1	5'-CTCGAGGCAAGGGACACACT-3'	5'-AAAGGACTCAGCCCTGAAGA-3'
Ifng	5'- CATTCAGAGCTGCAGTGACC-3'	5'- CTGTCTGGCCTGCTGTTAAA-3'
Il21	5'-GGCCATTCCCACTCCCATCT-3'	5'-TTCTGCGCACTGAGGAGAGG-3'
Cd40l	5'-AGGCGGCAAATACCCACAGT-3'	5'-TGGCTTGCTTCAGTCACGTTG-3'
Ccl21a	5'-GCTCCAAGGGCTGCAAGAGA-3'	5'-TTGCCTGTGAGTTGGACCGT-3'
Cxcl9	5'-TCTGCCATGAAGTCCGCTGT-3'	5'-GCAGGAGCATCGTGCATTCC-3'
Adipoq	5'- AAGGCCGTTCTCTTCACCTA-3'	5'-TACACCTGGAGCCAGACTTG-3'
Pparg	5'-TTCTGCGCACTGAGGAGAGG-3'	5'-AGACTCTGGGTTCAGCTGGT-3'
Ppara	5'-AGACTCTGGGTTCAGCTGGT-3'	5'-GAAGCTGGAGAGAGGGTGTC-3'
Rorα	5'-ACTTGCGGGAAGAGCTCCAG-3'	5'-CACACAGCTGCCACATCACC-3'

Note: Primer sets were designed at https://www.genscript.com/tools/real-time-pcr-taqman-primer-design-tool. The parameters used include the minimum Tm 58^{o}C, optimum Tm 59^{o}C, maximum Tm 60^{o}C, primer length 16-20 bp, amplicon size 90-150 bp. Primer crossing exon junction is not allowed. h=human.

3. Supplementary Materials and Methods

The details of other materials and methods used throughout the study include (1) Animal treatment; (2) Production of recombinant FGF21; (3) Cell culture; (4) Histology analysis; (5) Immunohistochemistry and immunofluorescence; (6) Analysis of FGF21 levels on human pancreatic tissue array; (7) Pancreatic fibrosis; (8) PanIN quantification; (9) Ki-67 proliferation index; (10) Protein isolation and Western blot analysis; (11) RAS activity assay; (12) Gene expression analysis; (13) Triglycerides content in the pancreas; (14) Pancreatic acini extraction and 3-dimensional culture; (15) Serum FGF21 levels; (16) Statistical analysis.

Animal treatment

fElas^{CreERT}, *fElas*^{CreERT};*Kras*$^{LSL\text{-}G12D/+}$, *Ptf1a*^{CreERT};*Kras*$^{LSL\text{-}G12D/+}$, and *fElas*^{CreERT};*Trp53*$^{LSL\text{-}R172H/+}$ mice, including both male and female, were randomly recruited and given TM by peritoneal injection for five consecutive days to fully activate Cre recombinase in acinar cells. According to the treatment plan, *Kras*$^{G12D/+}$ and *fElas*^{CreERT} mice were fed with either normal laboratory supplied diet or high-fat diet (60% fat, Test Diet DIO 58Y1 van Heek Series; Lab Supply, Fort Worth, TX). The mice were given rhFGF21 at 0.5 mg/kg/day as described[1, 2]. Phosphate-buffered saline (PBS) of the same volume was used as an experimental control. Body weight of each mouse was measured at least once a week. After about ten weeks of treatment or due to tumor burden requiring a humane sacrifice, mice were euthanized, and the pancreas, liver, spleen, blood, and/or fat tissues were harvested for further experiments.

Production of recombinant FGF21

Recombinant 6 x His-tagged human FGF21 for *in vivo* injection was produced in *E. coli* BL21 DE3 and purified as described[3].

Cell culture

Panc-1, MIA Paca-2, SU86.86, and AsPC-1 cells were cultured in RPMI 1640 or DMEM media supplemented with 10% FBS, as well as penicillin and streptomycin. All these cell lines were obtained from American Type Culture Collection (ATCC) and proven to carry oncogenic *KRAS.* HPDE cells were cultured in serum-free keratinocyte (KSF) medium supplemented by epidermal growth factor and bovine pituitary extract (Life Technologies, Inc., Grand Island, NY).

Histology analysis

Mouse tissues were dissected, rinsed with PBS, and fixed in 10% formalin solution overnight. Formalin-fixed tissue samples were placed in cassettes, dehydrated in alcohol gradients, and then embedded in paraffin for sectioning. The 5-μm-thick tissue sections were dewaxed in xylene, rehydrated through reversed ethanol gradients, washed in PBS thoroughly, and then stained with H&E. After staining, the pathological changes in pancreatic tissues were evaluated by our experienced pathologists based on criteria described at http://pathology.jhu.edu/pc/professionals/DuctLesions.php. PDAC incidences were also assessed by two independent pathologists.

Immunohistochemistry and immunofluorescence

To evaluate the levels of representative protein makers, including COX-2, FGF21, KLB, F4/80, Ki-67, Cyclin D1, amylase, CD3, and CK19, immunohistochemical and immunofluorescent analyses were performed as described[4, 5]. Briefly, after deparaffinized in xylene, rehydrated in alcohol gradients and rinsed with PBS, tissue sections were subjected to heat-mediated antigen retrieval with citrate buffer (pH 6.0) and then treated with 0.5% H_2O_2 in methanol for 10 min to remove the endogenous peroxidase followed by blocking with normal serum. The treated sections were then incubated with primary antibodies against COX-2 (1:20, Thermo), FGF21 (1:200, Abcam), KLB (1:200, Abcam), F4/80 (1:100, eBioscience), Ki-67 (1:200, Thermo), Cyclin D1 (1:200, Santa Cruz), amylase (1:400, Santa Cruz), and CK19 (1:50, Santa Cruz) at 4℃ overnight. After washing, the sections were further incubated with the appropriate biotinylated secondary antibodies (Vector Laboratories, CA, USA) at room temperature for 1 hr, washed again in PBS, incubated with ABC reagent (Vector Laboratories, CA, USA) for 30 min, and then reacted with diaminobenzidine (DAB, Vector Laboratories, CA, USA) for about 3 min. The resulting sections were then counterstained with hematoxylin until the desired stain intensity developed. Immunofluorescence was performed as described[4, 5]. Fiji ImageJ software was used to obtain data from most IHC images for quantification and statistical analyses.

Analysis of FGF21 levels on human pancreatic tissue array

Human normal (n=45) and PDAC (n=59) pancreatic tissue array samples (US Biomax, MD, USA) were processed for IHC analysis on FGF21 expression. Positive FGF21

expression was defined as the presence of cytoplasm staining in cells. Tissue cores containing tumor foci in less than 10% of the whole area were excluded from evaluation. Relative FGF21 levels were scored as the product of a proportion score and an intensity score. The proportion score was determined by the fraction of positively stained neoplastic cells (0, none; 1, <10%; 2, 10–50%; 3, 51–80%; 4, >80%). The intensity score represented the staining intensity (0 = negative, 1 = weak, 2 = moderate, 3 = strong). Mean staining intensity of three tumor cores per patient on the tissue array was calculated for each case.

Pancreatic fibrosis

To evaluate pancreatic fibrosis, we analyzed the levels of pancreatic collagen using Sirius Red staining on pancreatic tissue sections. Briefly, tissue sections were deparaffinized, hydrated in ethanol gradients and distilled water, and then incubated in adequate Picro-Sirius Red Solution (Abcam, MA, USA) for 60 minutes. After rinsing quickly in two changes of acetic acid solution followed by dehydration with two changes of absolute alcohol, the Sirius Red-stained sections were sealed and photographed under light microscopes. Three digitized pictures of each pancreatic section were photographed using an Olympus iX81 microscope at 200x magnification. The images were analyzed using Fiji ImageJ software. Levels of pancreatic collagen deposition were presented as the ratio of the mean collage-stained area to the whole mean area of the section and finally converted to relative collagen contents.

PanIN quantification

The H&E stained pancreatic sections were histologically evaluated by two independent pathologists blinded to the experimental groups according to histopathology criteria as recommended[6]. Each lobule of the pancreas on each section was examined, and the highest grade lesion from each lobule was identified, and the percentage of lobules with the highest grade of each type of lesion was determined based upon the total number of lobules counted.

Ki-67 proliferation index

Ki-67 proliferation index was determined as the percentage of positively stained cell nuclei of neoplastic cells. 5-10 random fields were chosen per tissue section (200x). Non-neoplastic cells such as lymphocytes and endothelial cells were excluded for counting[7].

Protein isolation and Western blot analysis

To evaluate protein levels of amylase, α-SMA, FGF21, KLB, GAPDH, and β-actin, cell and tissue lysates were separated by SDS-PAGE and analyzed by immunodetection as described[8]. Briefly, snap-frozen tissues were homogenized in 0.5-1 ml ice-cold lysis buffer (Millipore, MA, USA) with protease inhibitor cocktail tablets (Roche, Germany). Tissue homogenates were centrifuged at 15,000 g for 15 minutes at 4℃, and the supernatant was collected. Protein lysates from tissue were aliquoted to determine protein concentration using a protein assay dye reagent concentrate (Bio-Rad, CA, USA). The lysates were separated by SDS-PAGE and then transferred to nitrocellulose membranes [8]. The membranes were rinsed with PBS containing 0.05% Tween 20

(PBS-T) and probed with the following antibodies against amylase (1:20000; Santa Cruz Biotechnology Inc.), α-SMA (1:400; Abcam), FGF21 (1:1000; Abcam), KLB (1:2000, R&D), GAPDH (1:10,000; Sigma-Aldrich), and β-actin (1:10000, Sigma-Aldrich). The membranes were then washed with PBS-T and probed with the respective secondary antibodies conjugated to horseradish peroxidase or Alexa-Fluor 800 or 680 for one hour at room temperature. Autoradiography or the Odyssey Imaging System (LiCor Biosciences, Lincoln, NE) was used to visualize protein bands. Stripping buffer (Thermo, MA, USA) was used for sequential blotting and reprobing with other antibodies to provide a loading control. ImageJ densitometry software was used to quantify individual bands.

RAS activity assay

Levels of GTP-occupied RAS from mice pancreatic lysates were measured using a RAF pull-down assay kit (Millipore, MA, USA) as previously described[9]. Briefly, snap-frozen pancreatic tissues were homogenized on ice in lysis buffer. Cellular debris was removed by centrifuging at 15,000g for 20 minutes at 4℃. P rotein concentrations were measured. About 1000 µg of lysates were incubated for 50 minutes at 4℃ w ith agarose beads coated with RAF-RBD domain, which can specifically pull-down the GTP-bound form of Ras proteins. The beads were then washed for 3 times with washing buffer. Active RAS was analyzed by immunoblotting with an anti-RAS primary antibody (1:2000, Millipore) using GAPDH as a sample loading control. The intensity of the bands generated from Western blot assay was quantified using ImageJ software, and the fold changes relative to RAS activity from *fElas*^{CreERT} mice were determined.

Gene expression analysis

The gene expression of *Fgf21*, *Klb*, *Fgfr1,* multiple inflammatory cytokines (Inflammatory Cytokines and Receptors PCR Array, Qiagen) and multiple FGF21-regulating transcription factors relative to *β-actin* and *18S rRNA* (Supplementary Table 1) were analyzed by qRT-PCR. Total RNA isolation, 1st strand cDNA synthesis, semi-quantitative PCR, and qPCR were performed as described[8]. Briefly, tissues or cells were homogenized in 1 ml TRIzol Reagent (Ambion, Life Technologies, CA), total RNAs were further separated from other cell contents by sequential chloroform and isopropanol precipitation. Aliquots of RNA samples were quantified and examined before reverse transcription using a Nanodrop to verify that there was no contamination with protein and genomic DNA. Semi-quantitative RT-PCR products after 32 cycles were analyzed by agarose gel electrophoresis. Inflammatory cytokine gene arrays (Inflammatory Cytokines and Receptors PCR Array, Qiagen) were first used to determine by qRT-PCR the changes in gene expression of inflammatory cytokines/chemokines and receptors. Gene expressions of statistically significant alterations were then individually confirmed by qRT-PCR using primer sets as listed in Supplementary Table 1, in the Quantifast SYBR Green PCR mix (Qiagen GmbH, Germany) with a reaction condition of initial denaturation at 95^{o}C for 5 min and then 40 cycles of 95^{o}C for 10 seconds and 60^{o}C for 30 seconds in QuantStudio 3 machine. The comparative threshold Ct method was used with *β-actin* and *18S rRNA* as internal references. Data quantification and statistic analysis were performed in Microsoft Excel and GraphPad Prism 6.0.

PPARG activation and FGF21 expression

To evaluate the effect of PPARG activation on pancreatic *FGF21* expression, we utilized the mutant *KRAS*-harboring Panc-1 cells. These cells were freshly cultured in RPMI-1640 media containing 10% FBS in 6-well plates at equal cell density. When reaching subconfluent (about 80%), these cells were treated with Rosiglitazone at concentrations of 0, 0.1, 1, and 10 μM for 18 hours. Cells were washed once with warm 1 x PBS, and total RNA was extracted for qRT-PCR analysis as described above.

Triglycerides content in the pancreas

Triglyceride colorimetric assay kit (Cayman Chemical Company, MI, USA) was used to determine the triglycerides content in the pancreas. 500 mg of fresh pancreatic tissues were minced into small pieces and homogenized in 2 ml of diluted Standard Diluent containing protease inhibitor cocktail tablets (Roche, Germany). The homogenates were then centrifuged at 10,000 x g for 10 minutes at 4°C, and the supernatant was transferred to another tube. An appropriate volume of samples was added to the designated wells on the plate according to the protocol. Reactions were initiated by adding the corresponding diluted enzyme solution. After incubating for 15 minutes at room temperature, the absorbance of the reaction was determined at 530-550 nm on a plate reader.

Pancreatic acini extraction and 3-dimensional culture

Pancreatic acini were prepared as described previously[10], seeded in collagen containing 24-well plates, cultured, treated daily with rhFGF21 (1 μg/ml) or PBS, and stained with H&E or co-immunofluorescent probes as described[10-12]. Three independent experiments were performed.

Serum FGF21 levels

Mouse whole blood samples were collected in clean 1.5 ml Eppendorf centrifuge tubes. For rhFGF21 treatment groups, blood samples were collected 24 hrs after rhFGF21 injection. Tubes with blood samples were placed on ice for 30 min without any disturbance. Blood samples were then centrifuged at 3,000 rpm for 10 min at 4℃, and the supernatants were harvested and stored at −80℃ until analyzed. Serum FGF21 concentrations were measured using Rat/Mouse (#MF2100) FGF21 enzyme-linked immunosorbent assay (ELISA) kits (Quantikine ELISA; R&D Systems, Minneapolis, MN, USA).

Statistical analysis

Comparison between two groups was analyzed by Student's *t*-test unless otherwise indicated. Log-rank (Mantel-Cox) test, based on the Log-rank statistic, was performed to determine the significant differences between two or more survival curves. The body weight data were analyzed by two-way ANOVA Tukey's multiple comparisons test. *p* values of less than 0.05 were considered to be statistically significant. Results were expressed as group mean ± SEM or mean ± SD. *, $p<0.05$; **, $p<0.01$; ***, $p<0.001$; ****, $p<0.0001$. ns, not significant. We used GraphPad Prism 6.0 for statistical analysis.

References

1. Adams AC, Yang C, Coskun T, et al. The breadth of FGF21's metabolic actions are governed by FGFR1 in adipose tissue. Mol Metab 2012;2:31-7.
2. BonDurant LD, Ameka M, Naber MC, et al. FGF21 Regulates Metabolism Through Adipose-Dependent and -Independent Mechanisms. Cell Metab 2017;25:935-944 e4.
3. Yang C, Jin C, Li X, et al. Differential specificity of endocrine FGF19 and FGF21 to FGFR1 and FGFR4 in complex with KLB. PLoS One 2012;7:e33870.
4. Siveke JT, Einwachter H, Sipos B, et al. Concomitant pancreatic activation of Kras(G12D) and Tgfa results in cystic papillary neoplasms reminiscent of human IPMN. Cancer Cell 2007;12:266-79.
5. Kopp JL, von Figura G, Mayes E, et al. Identification of Sox9-dependent acinar-to-ductal reprogramming as the principal mechanism for initiation of pancreatic ductal adenocarcinoma. Cancer Cell 2012;22:737-50.
6. Hingorani SR, Petricoin EF, Maitra A, et al. Preinvasive and invasive ductal pancreatic cancer and its early detection in the mouse. Cancer Cell 2003;4:437-50.
7. Khan MS, Luong TV, Watkins J, et al. A comparison of Ki-67 and mitotic count as prognostic markers for metastatic pancreatic and midgut neuroendocrine neoplasms. Br J Cancer 2013;108:1838-45.

8. Lu W, Hu Y, Chen G, et al. Novel role of NOX in supporting aerobic glycolysis in cancer cells with mitochondrial dysfunction and as a potential target for cancer therapy. PLoS Biol 2012;10:e1001326.

9. Huang H, Daniluk J, Liu Y, et al. Oncogenic K-Ras requires activation for enhanced activity. Oncogene 2014;33:532-5.

10. Gruber R, Panayiotou R, Nye E, et al. YAP1 and TAZ Control Pancreatic Cancer Initiation in Mice by Direct Up-regulation of JAK-STAT3 Signaling. Gastroenterology 2016;151:526-39.

11. Qu C, Konieczny SF. Pancreatic Acinar Cell 3-Dimensional Culture. Bio Protoc 2013;3.

12. Shen J, Ha DP, Zhu G, et al. GRP78 haploinsufficiency suppresses acinar-to-ductal metaplasia, signaling, and mutant Kras-driven pancreatic tumorigenesis in mice. Proc Natl Acad Sci U S A 2017;114:E4020-E4029.

ACCEPTED MANUSCRIPT